


Stability of surfactant-laden liquid film flow over a cylindrical rod

Ashwin Nair and Gaurav Sharma*

Department of Chemical Engineering, Indian Institute of Technology Roorkee, Roorkee 247667, India (Received 19 May 2020; accepted 28 July 2020; published 19 August 2020)

The stability of surfactant-laden liquid film flow over a cylindrical rod is examined in creeping flow limit using standard temporal linear stability analysis. The clean film flow configuration (i.e., in absence of surfactant) is well-known to become unstable owing to Rayleigh-Plateau instability of cylindrical liquid interfaces. Previous studies demonstrated that for a static liquid film (i.e., zero basic flow) coating a rod, the presence of interfacial surfactant decrease the growth of Rayleigh-Plateau instability, but is unable to suppress it completely. Further, the presence of interfacial surfactant is known to introduce an additional mode, referred to as surfactant mode in the present work. To the best of our knowledge, the stability of surfactant mode has not been analyzed in the context of cylindrical film flows. Thus, we reexamined the stability of surfactant-laden cylindrical liquid film flow to analyze the stability behavior of the above said two modes when the basic flow is turned on. The present study reveals that the incorporation of basic flow in stability analysis leads to the complete suppression of Rayleigh-Plateau instability due to the presence of interfacial surfactants as compared to the partial suppression obtained for a stationary liquid film. Three nondimensional parameters appear for this problem: Bond number (denoted as Bo) which characterizes the strength of basic flow, Marangoni number (denoted as Ma) which signifies the presence of surfactant, and ratio of rod radius to film thickness denoted as S . In creeping flow limit, the characteristic equation is quadratic with one root belonging to Rayleigh-Plateau mode and the other to surfactant mode. We first carried out an asymptotic analysis to independently capture the eigenvalues corresponding to both the modes in limit of long-wave disturbances. The long-wave results show that the Rayleigh-Plateau instability is completely suppressed on increasing the Marangoni number above a critical value while the surfactant mode always remains stable in low wave-number limit. The continuation of long-wave results to arbitrary wavelength disturbances show that the suppression of Rayleigh-Plateau instability mode still holds, however, the surfactant mode becomes unstable at sufficiently high values of Marangoni number. Further, this surfactant mode instability shifts toward low wave numbers with critical Marangoni number for instability scaling with wave number in a particular fashion. We used this scaling and carried out an asymptotic analysis to capture this instability in low wave-number limit. Depending on S and Bo , we observed the existence of a stable gap in terms of Ma where both the eigen-modes remain stable. Our results indicate that for a given Bond number, the width of stable gap in terms of Ma decreases with decrease in S and the stable gap vanishes when S is sufficiently small. The effect of increasing Bond number (or equivalently, the strength of basic flow) is found to be stabilizing for the film flow configuration.

DOI: [10.1103/PhysRevE.102.023111](https://doi.org/10.1103/PhysRevE.102.023111)**I. INTRODUCTION**

The flow of a liquid film down a vertical cylindrical rod is important in several technological applications. Goren [1] carried out the linear stability analysis for a stationary liquid film coating a wire and demonstrated the presence of a surface-tension driven capillary instability similar to the classical Rayleigh-Plateau (RP) instability of a cylindrical liquid jet. Subsequent studies [2–4] incorporating the gravity-induced flow in the film demonstrated the appearance of an additional mechanism of instability due to the presence of free-surface. This free-surface instability is also present for a planar gravity-driven liquid film flow [5]; however, inertia is always required to trigger this free-surface instability (both for planar and cylindrical films). In contrast, the capillary in-

stability exhibited by cylindrical films exist even for stationary film and/or in Stokes' flow limit. In the present work, we are interested in examining the effect of interfacial surfactant on the capillary instability of a liquid film flow over a cylindrical rod, and thus, we analyze the problem in creeping flow limit to eliminate the possibility of free-surface instability.

There are lot of theoretical and experimental studies exploring the nonlinear dynamics and evolution of film once the Rayleigh-Plateau or capillary instability sets in for a liquid film coating a cylindrical rod [6–18]. However, relatively less attention is paid to study the effect of presence of surfactant at air-liquid interface on cylindrical film stability. Even among those, most of the efforts have been directed toward understanding the effect of surfactant on the stability of liquid film lining the inside of a tube because of the relevance of this inside configuration to lung airway closure mechanism. For the inside film configuration, the presence of surfactant reduces the growth rate of RP instability but cannot suppress

*gaurav.sharma@ch.iitr.ac.in

it completely [19–22]. A similar conclusion regarding the reduced growth rate has also been made by Carroll and Lucassen [23] for surfactant-laden liquid film coated outside of a cylindrical fiber. In fact, the growth rate reduces by a maximum factor of 4 for both inside [19] and outside [23] surfactant-laden film as compared with the growth rate for a clean film.

All the above cited studies related to reduction of growth rate of RP capillary instability due to the presence of surfactant assumed a static liquid film, and ignored the effect of presence of gravity-driven basic flow. To the best of our knowledge (and surprisingly), we could not find any study which evaluates the role of surfactants for liquid film coating a cylindrical rod while taking into account of the presence of basic flow. The role of basic flow in suppressing the free-surface instability due to the presence of interfacial surfactants for a planar liquid film has been highlighted by Wei [24]. There are other instances as well where a flow-induced stabilization of interfacial instabilities has been achieved, for example, in core-annular flows in rigid [25] and flexible tubes [26]. Thus, we carry out a careful, standard temporal linear stability analysis for surfactant-laden film flow coating on the exterior of a cylindrical rod by taking into account of the presence of basic flow. We show that while complete suppression is not possible for a stationary film, the RP capillary instability completely vanishes due to the presence of surfactant when basic flow is turned on.

Another point worth mentioning is the introduction of a mode of instability in addition to already present capillary instability mode due to the presence of an interfacial surfactant. Halpern and Frenkel [27,28] were the first to uncover the instability of this surfactant induced additional mode in long-wave disturbance limit for two-layer channel flow (even) in Stokes' flow limit. This surfactant induced mode is referred to as Marangoni/surfactant mode in literature. Blyth and Pozrikidis [29] demonstrated that the Marangoni mode remains stable for surfactant-laden liquid film flowing down an incline plane for all wave numbers. The Marangoni mode was also never observed to become unstable for cylindrical fluid-fluid interfaces, for example in core-annular or rod-annular flow configurations [30–32] or for simple liquid thread. In direct relevance to the present work, Carroll and Lucassen [23] examined the stability of surfactant-laden stationary liquid film coating a vertical fiber. However, they focused on the effect of surfactant on Rayleigh-Plateau instability, and did not make any mention of the stability of surfactant mode. Probably due to Marangoni mode remaining stable for flow configurations involving cylindrical fluid-fluid interfaces and for planar-free surface flows, the stability of Marangoni mode for film coating a rod has not received any attention. Here, we examined the stability of Marangoni mode for film flow over a vertical rod, and show that this mode remains stable in long-wave disturbance limit, however, when the results corresponding to Marangoni mode are continued from long-wave (or low-wave-number) limit to finite wave numbers, we observe that a band of wave numbers become unstable at sufficiently high Marangoni number. This observation is in contrast to earlier studies related to free surface flows where the Marangoni mode in low-wave-number limit and its continuation to finite wave numbers was always found to

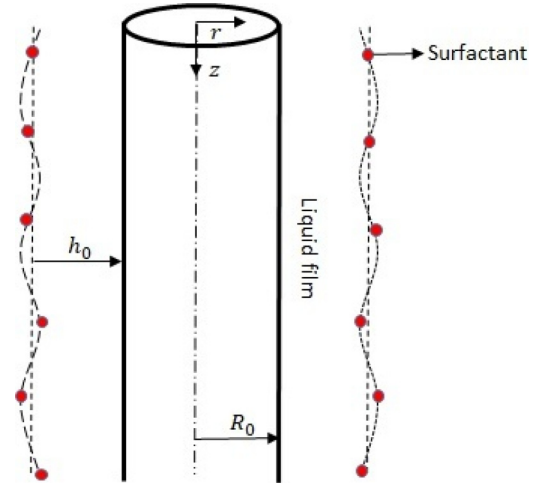


FIG. 1. Surfactant-laden Newtonian liquid film flowing outside a rigid vertical cylinder.

be stable. However, we show in the end that the instability observed here at higher Marangoni number is not the true surfactant/Marangoni mode because it requires fluctuations in both surfactant concentration and gas-liquid interfacial location for its existence. In contrast to this, earlier studies related to film flows [29,33] identified Marangoni/surfactant mode on the basis of presence of disturbances only in surfactant concentration without necessarily having fluctuations in gas-liquid interfacial location. We further show that this instability observed at high Marangoni number shows connection with RP capillary instability in the limit of zero basic flow. In context of the above discussion, it is also important to note that the presence of surfactant was also found to have a destabilizing effect on capillary mode for the core-annular flow in a horizontal pipe [30]. Also, these previous studies related to core-annular or rod-annular flows [30–32] used Marangoni number values as unity or less than unity in presenting their results.

Based on the literature, in the present work, we carry out a careful examination of both RP and Marangoni mode instabilities for surfactant-laden film flow coating on a vertical cylindrical rod. The rest of the paper is organized as follows: Section II describes the flow configuration and presents the equations governing the linear stability of the film flow problem. Section III discusses the solution procedure, and more importantly, explains the procedure that we follow to identify the eigenvalues as either belonging to RP or surfactant mode. Section IV presents the long-wave asymptotic analysis to capture the eigenvalues corresponding to both RP and surfactant modes. The results for arbitrary wavelength disturbances are discussed in Sec. V, and finally we summarize our finding in Sec. VI.

II. PROBLEM FORMULATION

We consider a Newtonian liquid film (of density ρ , and viscosity μ) falling down a vertical cylindrical rod/fiber (of radius R_0) under the action of gravity (Fig. 1). The unperturbed thickness of the liquid film is h_0 , and the film is in contact with a passive gas. The gas-liquid interface is

covered with a monolayer of insoluble surfactant with local surface concentration of surfactant denoted by $\Gamma^*(z^*, t^*)$. The surfactant can convect and diffuse along the gas-liquid (GL) interface to locally alter the surface tension according to the simple linear relationship: $\gamma^*(z^*, t^*) = \gamma_0^* - E(\Gamma^*(z^*, t^*) - \Gamma_0^*)$, where Γ_0^* is the surfactant concentration in unperturbed state, γ_0^* is the interfacial tension corresponding to undisturbed surfactant concentration Γ_0^* , and $E = -(\frac{\partial \gamma^*}{\partial \Gamma^*})_{\Gamma_0^*}$ is surface elasticity. Further, we assume negligible diffusion of surfactant along the GL interface and fix diffusion coefficient $D_s = 0$ in the present study. As mentioned in the Introduction we are interested in analyzing the problem in creeping flow limit, therefore, the governing equations for the flow in liquid film are

$$\nabla^* \cdot \mathbf{v}^* = 0, \quad \nabla^* \cdot \mathbf{T}^* + \rho \mathbf{g}^* = \mathbf{0}, \quad (1)$$

where, $\mathbf{T}^* = -p^* \mathbf{I} + \mu[\nabla^* \mathbf{v}^* + (\nabla^* \mathbf{v}^*)^T]$ is the total stress tensor, \mathbf{v}^* and p^* are, respectively, the velocity and pressure fields. The GL interface in perturbed state is located at $r^* = h^*(z^*, t^*) = h_0 + h'(z^*, t^*)$. The stress balance equation at GL interface in the presence of surfactant is [34]

$$(\mathbf{n} \cdot \mathbf{T}^*) = \nabla_s^* \gamma^* - \gamma^* \mathbf{n} (\nabla^* \cdot \mathbf{n}), \quad (2)$$

where, \mathbf{n} is the unit normal vector pointing from liquid to gas phase, and $\nabla_s^* = \nabla^* - \mathbf{n}(\mathbf{n} \cdot \nabla^*)$ is the surface gradient operator. The normal stress balance is obtained by taking an inner product of Eq. (2) with \mathbf{n} and this gives: $(\mathbf{n} \cdot \mathbf{T}^* \cdot \mathbf{n}) = -\gamma^* (\nabla^* \cdot \mathbf{n})$. This condition implies that the normal component of stress is balanced by the surface tension force, and in the limiting case of static liquid film, it reduces to Young-Laplace pressure jump condition [34]. The tangential component of stress is obtained by taking a dot product of Eq. (2) with tangent vector \mathbf{t} . The tangential stress balance is then written as $(\mathbf{n} \cdot \mathbf{T}^* \cdot \mathbf{t}) = (\nabla_s^* \gamma^*) \cdot \mathbf{t}$. This equation shows that the Marangoni stress induced by gradient of surface tension (right-hand-side term) is balanced by tangential stress in liquid film. Note that the surface tension gradient can occur because of the variation in surfactant concentration along the GL interface, and hence, the Marangoni stresses are expected to affect the stability of the present film flow configuration. The equation governing the transport of surfactant species at GL interface under the assumption of negligible diffusion coefficient, $D_s = 0$, is $\frac{\partial \Gamma^*}{\partial t^*} + \nabla_s^* \cdot \mathbf{v}^* = 0$ [34–36]. On expressing \mathbf{v}^* in terms of component of velocity along the interface [i.e., $\mathbf{v}_s^* = \mathbf{v}^* - (\mathbf{v}^* \cdot \mathbf{n})\mathbf{n}$], we obtain the surfactant transport equation as

$$\frac{\partial \Gamma^*}{\partial t^*} + \nabla_s^* \cdot (\Gamma^* \mathbf{v}_s^*) + \Gamma^* (\nabla_s^* \cdot \mathbf{n})(\mathbf{v}^* \cdot \mathbf{n}) = 0. \quad (3)$$

The above equation shows that there are two contributions that change the local surfactant concentration [first term in Eq. (3)]: convection of surfactant species with interface velocity \mathbf{v}_s^* represented by second term in above equation, and third term representing the change in Γ^* due to local change in interfacial area. The kinematic condition for the evolution of GL interface is $\partial_{t^*} h^* + v_z^* \partial_{z^*} h^* = v_r^*$. Finally, the velocity field satisfies no-slip and no-penetration conditions ($\mathbf{v} = 0$) at $r^* = R_0$.

We use the following scales to nondimensionalize different variables: h_0 for lengths, γ_0^*/μ for velocities, γ_0^*/h_0 for stresses and pressure, Γ_0^* for surfactant concentration, and γ_0^* for surface tension. As a result of nondimensionalization, three dimensionless parameters appear in the problem:

$$S = \frac{R_0}{h_0}, \quad \text{Bo} = \frac{\rho g h_0^2}{\gamma_0^*}, \quad \text{Ma} = \frac{E \Gamma_0^*}{\gamma_0^*}. \quad (4)$$

Here, S is the ratio of rod radius to film thickness, Bo is Bond number, and Ma is the Marangoni number. Note that $\text{Ma} = 0$ recovers the clean film case, i.e., when the film is devoid of surfactant species.

The basic flow consists of one-dimensional, laminar, steady state solution of Navier-Stokes equation when the gas-liquid interface remains perfectly cylindrical and free of any interfacial perturbations. The nonzero component of velocity, under the above mentioned assumptions, is \bar{v}_z^* which depends only on radial coordinate r^* . The expression of \bar{v}_z^* is obtained by solving the simplified z -component of Navier-Stokes equation along with appropriate boundary conditions [37]:

$$\begin{aligned} \frac{\mu}{r^*} \frac{d}{dr^*} (r^* \frac{d\bar{v}_z^*}{dr^*}) + \rho g = 0, \quad \bar{v}_z^*(r^* = R_0) = 0, \\ \mu \frac{d\bar{v}_z^*}{dr^*} = 0 \quad @ r^* = R_0 + h_0. \end{aligned} \quad (5)$$

The pressure profile is obtained from simplified r -component Navier-Stokes equation ($\frac{dp^*}{dr^*} = 0$) along with normal stress balance at gas-liquid interface ($p^* - p_g^* = \frac{\gamma_0^*}{R_0 + h_0}$). Here, p_g^* is constant pressure in passive gas region. The velocity profile and pressure distribution thus obtained is then made dimensionless using the above mentioned scales. Finally, the dimensionless basic velocity profile and pressure distribution are given as

$$\begin{aligned} \bar{v}_z(r) = \frac{\text{Bo}}{4} \left[S^2 - r^2 + 2(S+1)^2 \ln\left(\frac{r}{S}\right) \right], \\ \bar{p}(z) = p_g + \frac{1}{S+1}. \end{aligned} \quad (6)$$

A standard temporal linear stability analysis is carried out in which all the dynamical variables (interfacial location, velocities, pressure, and surfactant concentration) are perturbed about their basic state value: $g = \bar{g} + g'$, where g represents any dynamical variable. \bar{g} is the base state value, and g' is the axisymmetric disturbance which is represented in terms of Fourier modes as: $g' = \tilde{g}(r) \exp[ik(z - ct)]$. Here, $\tilde{g}(r)$ is the complex amplitude of the disturbance, k is the real wave number of perturbations, and $c = c_r + ic_i$ is the complex wave speed. If $c_i > 0$ (or $c_i < 0$), then flow will be unstable (or stable). On substitution of above form of perturbed variables in governing equations and retaining linear terms in perturbation variables, we obtain the linearized stability equations for liquid film falling down a cylindrical rod:

$$d_r \tilde{v}_r + \frac{\tilde{v}_r}{r} + ik \tilde{v}_z = 0, \quad (7)$$

$$-d_r \tilde{p} + [d_r^2 + r^{-1} d_r - r^{-2} - k^2] \tilde{v}_r = 0, \quad (8)$$

$$-ik \tilde{p} + [d_r^2 + r^{-1} d_r - k^2] \tilde{v}_z = 0, \quad (9)$$

where, $d_r = \frac{d}{dr}$. The linearized kinematic condition, tangential stress balance, normal stress balance, and surfactant transport equation at unperturbed GL interface ($r = S + 1$) are

$$ik[\bar{v}_z - c]\tilde{h} = \tilde{v}_r, \quad (10)$$

$$ik\tilde{v}_r + d_r\tilde{v}_z + \tilde{h}(d_r^2\tilde{v}_z) + ik\text{Ma}\tilde{\Gamma} = 0, \quad (11)$$

$$\tilde{p} - 2d_r\tilde{v}_r + \tilde{h}\left(\frac{1}{(S+1)^2} - k^2\right) + \frac{\text{Ma}\tilde{\Gamma}}{S+1} = 0, \quad (12)$$

$$[ik\{\bar{v}_z - c\}]\tilde{\Gamma} = d_r\tilde{v}_r. \quad (13)$$

Finally, the no-slip and no-penetration conditions at $r = S$ are

$$\tilde{v}_z = 0, \quad \tilde{v}_r = 0. \quad (14)$$

III. SOLUTION PROCEDURE AND MODE IDENTIFICATION

The linear stability of the flow configuration is governed by Eqs. (7)–(14). These equations are solved to determine the dispersion relation: $c = F(S, \text{Bo}, \text{Ma}, k)$. Equations (7)–(9) can be recast into a single fourth-order ordinary differential equation (ODE) in terms of \tilde{v}_r by substituting \tilde{v}_z from Eq. (7) and \tilde{p} from Eq. (9) in Eq. (8). The general solution of this fourth-order ODE is

$$\tilde{v}_r = C_1 r I_0(kr) + C_2 I_1(kr) + C_3 r K_0(kr) + C_4 K_1(kr). \quad (15)$$

Here, coefficients $\{C_1, C_2, C_3, C_4\}$ are integration constants, I_α and K_α are the modified Bessel function of first and second kind, respectively. The variables \tilde{v}_z and \tilde{p} are evaluated using Eqs. (7) and (9). The interfacial deflection \tilde{h} is calculated using Eq. (10), and surfactant concentration $\tilde{\Gamma}$ is calculated from Eq. (13) using the expression of \tilde{v}_r . All the expressions ($\tilde{v}_r, \tilde{p}, \tilde{v}_z, \tilde{h}, \tilde{\Gamma}$) are substituted in boundary conditions Eqs. (11), (12), and (14) to obtain a set of four linear homogeneous algebraic equations containing four unknown constant coefficients $\{C_1, C_2, C_3, C_4\}$. The determinant of coefficient matrix is equated to zero which yields a quadratic characteristic equation in eigenvalue c . Thus, we obtain two roots for c , say root-1 and root-2. It is important to mention here that the characteristic equation remains quadratic for both a surfactant-free film ($\text{Ma} = 0$), and a surfactant-laden film ($\text{Ma} \neq 0$). We used symbolic package MATHEMATICA to carry out the analytical calculations outlined above. Further, a multivariable Newton-Raphson method is used to evaluate the neutral stability curves in Ma versus k plane. We next discuss the procedure followed to identify and label the two roots as RP or surfactant mode.

It is well known that a surfactant-free cylindrical film is unstable due to a surface tension driven RP instability [4], and the presence of interfacial surfactant introduces a surfactant/Marangoni mode [27] in addition to already present RP mode. Both of these modes (RP and surfactant modes) can be captured and identified in long-wave disturbance regime by carrying out an asymptotic analysis in $k \ll 1$ limit. Thus, we examine the behavior of root-1 and root-2 in long-wave (or low-wave-number) limit to identify which among the two roots correspond to RP or surfactant mode. We observed that for $\text{Ma} = 0$, one of the root (say root-1) is a complex number while the second root (root-2)

is purely real. The real root-2 found to be equal to the base velocity at GL interface, i.e., $\bar{v}_{z@r=S+1}$ for $k \ll 1$. Since this root is real, it represents a pseudostable mode present for the surfactant-free film. However, the real part of root-1 is found to be equal to $2\bar{v}_{z@r=S+1}$, and the imaginary part is always found to be positive in low- k limit. Thus, this root-1 represents a traveling wave perturbation with positive growth rate, or equivalently, an unstable root for the surfactant-free film flow configuration. Since a surfactant-free film is known to become unstable due to RP instability mechanism, therefore, this root-1 is referred to as RP instability mode while root-2 is simply a pseudostable mode for $\text{Ma} = 0$ case. We next track the progress of these two roots as Ma is gradually increased above zero. For small and $\text{Ma} \neq 0$ (e.g., $\text{Ma} = 10^{-3}, 10^{-2}$ etc.), we observe that real part of root-1 (which corresponds to RP mode when $\text{Ma} = 0$) is still equal to $2\bar{v}_{z@r=S+1}$, while the imaginary part modifies slightly indicating a dependence on nonzero Marangoni number. The imaginary part of root-1 is still positive implying that root-1 is still an unstable root of the characteristic equation (for small Ma). These observations suggest that root-1 still corresponds to RP instability mode for surfactant-laden cylindrical films. Interestingly, an imaginary part starts to appear for root-2 at small and nonzero Marangoni numbers. Thus, root-2 becomes a complex quantity for $\text{Ma} \neq 0$ and the real part is still observed to remain identical to $\text{Ma} = 0$ case (i.e., $= \bar{v}_{z@r=S+1}$). As the presence of surfactant is known to introduce an additional normal mode referred to as surfactant/Marangoni mode [27,28], we identify this root-2 as surfactant/Marangoni mode. The imaginary part of this root is observed to be negative, and hence, this root-2 or surfactant mode remains a stable eigenmode in low-wave-number limit. As mentioned above that both RP and surfactant modes can be captured in long-wave disturbance limit, thus, we carry out a low-wave-number asymptotic analysis in next section to capture these two eigenmodes. A comparison of results obtained from the low- k analysis and the two roots obtained using the general characteristic equation again confirms that root-1 corresponds to RP mode and root-2 corresponds to Marangoni mode.

IV. LOW-WAVE-NUMBER ASYMPTOTIC ANALYSIS

In this section, we present a low-wave-number (or long-wavelength) asymptotic analysis to capture the eigenvalues corresponding to RP and surfactant mode in $k \ll 1$ limit. Specifically, we focus on two aspects: (i) how the presence of surfactant affects the stability of RP mode in presence of flow, and (ii) whether the surfactant/Marangoni mode become unstable or not in low- k limit? The complex wave speed is expanded as: $c = c^{(0)} + kc^{(1)} + \dots$ for $k \ll 1$. Here $c^{(0)}$ and $c^{(1)}$ are leading-order and first correction to wave speed, respectively. All the dimensionless parameters S, Ma , and Bo are assumed to be $O(1)$ quantity which implies that these parameters do not show any scaling with wave number. Further, the basic velocity profile is written as

$$\bar{v}_z(r) = \frac{\text{Bo}}{4} f(r), \text{ where } f(r) = \left[S^2 - r^2 + 2(S+1)^2 \ln\left(\frac{r}{S}\right) \right]. \quad (16)$$

If we set $\tilde{v}_r \sim O(1)$, then this implies $\tilde{v}_z \sim O(1/k)$ and $\tilde{p} \sim O(1/k^2)$ from Eqs. (7) and (9), respectively. Similarly,

$\tilde{h} \sim O(1/k)$ and $\tilde{\Gamma} \sim O(1/k)$ from Eqs. (10) and (13), respectively. All the variables are then expanded according to their respective scaling:

$$\begin{aligned} & \{ \tilde{v}_r, \tilde{v}_z, \tilde{p}, \tilde{h}, \tilde{\Gamma}, \} \\ & = \left\{ \tilde{v}_r^{(0)}, \frac{1}{k} \tilde{v}_z^{(0)}, \frac{1}{k^2} \tilde{p}^{(0)}, \frac{1}{k} \tilde{h}^{(0)}, \frac{1}{k} \tilde{\Gamma}^{(0)}, \right\} \\ & + k \left\{ \tilde{v}_r^{(1)}, \frac{1}{k} \tilde{v}_z^{(1)}, \frac{1}{k^2} \tilde{p}^{(1)}, \frac{1}{k} \tilde{h}^{(1)}, \frac{1}{k} \tilde{\Gamma}^{(1)} \right\} + \dots \end{aligned} \quad (17)$$

These expansions in Eq. (17) are substituted in governing equations and boundary conditions Eqs. (7)–(14), and the resulting set of equations are solved at each order in k . The equations at leading order are

$$d_r \tilde{v}_r^{(0)} + \frac{1}{r} \tilde{v}_r^{(0)} + i \tilde{v}_z^{(0)} = 0, \quad (18)$$

$$d_r \tilde{p}^{(0)} = 0, \quad (19)$$

$$i \tilde{p}^{(0)} - d_r^2 \tilde{v}_z^{(0)} - \frac{1}{r} d_r \tilde{v}_z^{(0)} = 0. \quad (20)$$

The above equations can be recast into a single fourth order differential equation in $\tilde{v}_r^{(0)}$:

$$d_r^4 \tilde{v}_r^{(0)} + \frac{2}{r} d_r^3 \tilde{v}_r^{(0)} - \frac{3}{r^2} d_r^2 \tilde{v}_r^{(0)} + \frac{3}{r^3} d_r \tilde{v}_r^{(0)} - \frac{3}{r^4} \tilde{v}_r^{(0)} = 0. \quad (21)$$

The tangential stress balance, normal stress balance, kinematic condition, and surfactant transport equations at leading order (at $r = S + 1$) are

$$d_r \tilde{v}_z^{(0)} + \tilde{h}^{(0)} (d_r^2 \tilde{v}_z) = 0, \quad (22a)$$

$$\tilde{p}^{(0)} = 0, \quad (22b)$$

$$\tilde{v}_r^{(0)} - i(\tilde{v}_z - c^{(0)}) \tilde{h}^{(0)} = 0, \quad (22c)$$

$$d_r \tilde{v}_r^{(0)} - i(\tilde{v}_z - c^{(0)}) \tilde{\Gamma}^{(0)} = 0. \quad (22d)$$

The leading-order velocity field satisfies no-slip conditions at rigid solid boundary:

$$\tilde{v}_z^{(0)} = 0, \quad \tilde{v}_r^{(0)} = 0. \quad (23)$$

The solution to Eq. (21) satisfying conditions Eqs. (22a), (22b), and (23) is

$$\tilde{v}_r^{(0)} = \frac{i \tilde{h}^{(0)} (1+S)}{4} \frac{1}{r} \left[S^2 - r^2 + 2r^2 \ln \frac{r}{S} \right] \tilde{v}_z'', \quad (24)$$

where, $\tilde{v}_z'' = d_r^2 \tilde{v}_z |_{r=S+1}$. Substituting leading-order velocity field [Eq. (24)] in kinematic condition [Eq. (22c)] and surfactant transport Eq. (22d), we obtain

$$\frac{i}{4} \tilde{h}^{(0)} f \tilde{v}_z'' - i(\tilde{v}_z |_{r=S+1} - c^{(0)}) \tilde{h}^{(0)} = 0, \quad (25)$$

$$\frac{i}{4} \tilde{h}^{(0)} \frac{A_1}{(S+1)} \tilde{v}_z'' - i(\tilde{v}_z |_{r=S+1} - c^{(0)}) \tilde{\Gamma}^{(0)} = 0, \quad (26)$$

where, $f = f(r) |_{r=S+1}$. The above set of equations [Eqs. (25) and (26)] admits two solutions for leading-order wave speed: one for $\tilde{h}^{(0)} \neq 0$, and second for $\tilde{h}^{(0)} = 0$ but with $\tilde{\Gamma}^{(0)} \neq 0$. When $\tilde{h}^{(0)} \neq 0$, the kinematic Eq. (25) yields the value of $c^{(0)}$ for RP mode and the surfactant transport Eq. (26) gives the

relationship between surfactant concentration and interfacial deflection,

$$c_{\text{RP}}^{(0)} = \bar{v}_z @_{r=S+1} - \frac{f}{4} \tilde{v}_z'' = 2 \bar{v}_z @_{r=S+1}, \quad (27)$$

$$\tilde{\Gamma}^{(0)} = \tilde{h}^{(0)} \left[\frac{A_1}{(S+1)f} \right], \quad (28)$$

where A_1 is a function of S given in Appendix B. It is important to point out here that while evaluating $\tilde{\Gamma}^{(0)}$ using Eq. (26), there occurs a cancellation of term $\tilde{v}_z'' (= -\text{Bo})$ from numerator and denominator. Thus, the expression of $\tilde{\Gamma}^{(0)}$ given above is valid only for nonzero Bond numbers. Since, $\tilde{\Gamma}^{(0)}$ is used in further calculations, the analysis that follow is strictly valid for $\text{Bo} \neq 0$. Note that the terms proportional to Ma in tangential and normal stress balances [Eqs. (11) and (12)], which accounts for the presence of surfactant, are absent in leading-order stress balance equations [Eqs. (22a) and (22b)]. Thus, the leading-order wave speed is exactly identical to the leading-order wave speed obtained for a clean film flowing down a rigid rod [29,33]. However, the interfacial deflection at GL interface causes a fluctuation in surfactant concentration at leading order as shown by Eq. (28). This leading-order surfactant concentration disturbance creates a surface tension gradient at GL interface, and hence, it is expected that the first correction to wave speed for RP mode could be modified by the presence of surfactant.

The second mode which exists purely because of fluctuation in surfactant concentration without necessarily having a perturbation in GL interfacial location ($\tilde{\Gamma}^{(0)} \neq 0$ and $\tilde{h}^{(0)} = 0$) is referred to as Marangoni/Surfactant mode. The leading-order wave speed from surfactant transport Eq. (26) for this mode is

$$c_{\text{Ma}}^{(0)} = \bar{v}_z @_{r=S+1}. \quad (29)$$

Note that since $\tilde{h}^{(0)} = 0$, the liquid layer admits a zero flow solution at leading order for Marangoni mode. Since, the leading-order wave speeds for both the modes are real, therefore, we cannot determine the stability of the system at this order and it is required to carry out calculations for next order in k .

The continuity and momentum equations can be written at $O(k)$ and can be combined into a single fourth-order ODE in $\tilde{v}_r^{(1)}$. This fourth-order ODE and boundary conditions at $O(k)$ are

$$d_r^4 \tilde{v}_r^{(1)} + \frac{2}{r} d_r^3 \tilde{v}_r^{(1)} - \frac{3}{r^2} d_r^2 \tilde{v}_r^{(1)} + \frac{3}{r^3} d_r \tilde{v}_r^{(1)} - \frac{3}{r^4} \tilde{v}_r^{(1)} = 0, \quad (30)$$

$$d_r \tilde{v}_z^{(1)} + (d_r^2 \tilde{v}_z) \tilde{h}^{(1)} + i \text{Ma} \tilde{\Gamma}^{(0)} = 0, \quad (31a)$$

$$\tilde{p}^{(1)} + \frac{1}{(S+1)^2} \tilde{h}^{(0)} + \frac{1}{(S+1)} \text{Ma} \tilde{\Gamma}^{(0)} = 0, \quad (31b)$$

$$\tilde{v}_z^{(1)} = 0, \quad \tilde{v}_r^{(1)} = 0, \quad (31c)$$

$$\tilde{v}_r^{(1)} - i(\tilde{v}_z - c^{(0)}) \tilde{h}^{(1)} + i c^{(1)} \tilde{h}^{(0)} = 0, \quad (31d)$$

$$d_r \tilde{v}_r^{(1)} - i(\tilde{v}_z - c^{(0)}) \tilde{\Gamma}^{(1)} + i c^{(1)} \tilde{\Gamma}^{(0)} = 0. \quad (31e)$$

The above system of equations is solved for first correction to wave speed for both RP and Marangoni mode.

A. The Marangoni/surfactant mode

The leading-order velocity field is absent for $\tilde{h}^{(0)} = 0$ and $\tilde{\Gamma}^{(0)} \neq 0$. This gives $c_{\text{Ma}}^{(0)} = \bar{v}_{z@r=S+1}$ from leading-order surfactant transport equation [Eq. (22d)]. The first correction to velocity field is then obtained by integrating Eq. (30) and using conditions given in Eqs. (31a)–(31c). The kinematic condition [Eq. (31d)] reduces to $\tilde{v}_r^{(1)}|_{S+1} = 0$ and this equation is used to determine the expression of $\tilde{\Gamma}^{(0)}$. This expression of $\tilde{\Gamma}^{(0)}$ is utilized in surfactant transport equation at $O(k)$ to determine the first correction to wave speed for Marangoni mode. The eigenvalue for surfactant/Marangoni mode is then given as

$$c_{\text{Ma}} = \bar{v}_{z@r=S+1} - ik\zeta\text{Ma}, \quad (32)$$

where ζ is a positive-valued function of S given in Appendix B. We have verified that the above equation shows excellent match with root-2 discussed in Sec. III. This expression for c_{Ma} shows that the Marangoni mode remains stable in low- k limit. This observation is consistent with several previous studies which state that shear stress exerted at fluid-fluid interface due to basic flow is required to trigger Marangoni mode instability [27,33]. Since the gas-liquid interface in the present film flow configuration remains stress free, the Marangoni mode does not become unstable.

B. Rayleigh-plateau instability mode

The governing Eq. (30) is solved for $\tilde{v}_r^{(1)}$ using conditions Eqs. (31a)–(31c), leading-order wave speed $c_{\text{RP}}^{(0)}$ [Eq. (27)], and relation between $\tilde{h}^{(0)}$ and $\tilde{\Gamma}^{(0)}$ [Eq. (28)]. The first correction to wave speed ($c_{\text{RP}}^{(1)}$) is then determined using kinematic condition at $O(k)$ [Eq. (31d)]. The $c_{\text{RP}}^{(1)}$ is found to be imaginary, and hence, the stability of RP mode can be established at $O(k)$. The above procedure gives the eigenvalue for RP mode correct up to $O(k)$:

$$c_{\text{RP}} = c_{\text{RP}}^{(0)} + kc_{\text{RP}}^{(1)} = 2\bar{v}_{z@r=S+1} + ik[q - n\text{Ma}], \quad (33)$$

where q and n are positive valued functions of $S(=R/h_0)$ and their expressions are given in Appendix B. We have verified that $q \rightarrow 0$ and $n \rightarrow 1$ as $S \rightarrow \infty$ in the Eq. (33) which recovers the case of surfactant-laden planar film flow in creeping flow limit [29,33,38]. The circumferential curvature $[1/(S+1)]$ decreases with increase in S , and approaches zero for large enough values of S , thus, recovering the planar film flow limit at large S . Also, the RP instability caused due to surface tension mainly arise from the circumferential curvature of the gas-liquid interface [39,40]. Since, this circumferential curvature is nonexistent for planar film flows, the RP capillary instability remains absent (i.e., $q \rightarrow 0$) for (clean or surfactant-laden) planar film flow past an inclined/vertical plane. The expression of c_{RP} matches very well with root-1 (refer Sec. III) in the limit of long-wave disturbances.

The first term in the imaginary part of eigenvalue c_{RP} (i.e., q) corresponds to the RP capillary instability exhibited by a clean stationary liquid film (i.e., for $\text{Ma} = 0$, and $\text{Bo} = 0$). This point can be verified by looking at the expression of RP mode eigenvalue obtained from a low- k zero-flow analysis given below [refer to Eq. (34)]. The second term proportional to Ma represents the effect of surfactant on RP instability. The

second term appears with a negative sign demonstrating the stabilizing effect of surfactant on RP instability mode. The above expression shows that the capillary instability is suppressed above a critical Marangoni number given by: $\text{Ma}_{\text{crit}} = q/n$. This finding is in stark contrast with the following general observation made in several previous studies: Even though partial stabilization of RP capillary mode is possible in presence of surfactants, a complete suppression of capillary instability using a mono-layer of surfactant is not possible for cylindrical liquid film flows [19,23]. As mentioned in the Introduction, these previous works calculated the growth rates (or equivalently eigenvalues) in the limit of thin stationary liquid coating. Thus, the basic flow was absent in these earlier studies. In contrast, the expression of c_{RP} given above is obtained when the base flow is nonzero. Thus, we anticipate that the complete stabilization observed above is a result of inclusion of the basic flow in the analysis. Recall that we have mentioned previously that the eigenvalue obtained above in Eq. (33) is not valid for $\text{Bo} = 0$ or in absence of flow. At this point, it is worth noting that both q and n are functions of S only, and are independent of strength of basic flow (characterized by Bo), thus, the nondimensional growth rate ($kc_i = k^2 c_{\text{RP}}^{(1)}$) and Ma_{crit} do not depend on Bond number. Such nondependence of growth-rate on Bond number has also been mentioned previously by Halpern and Wei [41] who examined the dynamics of clean liquid film falling down a vertical fiber. Zhou [42] also demonstrated that the growth-rate does not depend on Bond number for surfactant-laden liquid film flow inside of a tube. While the expression of $c_{\text{RP}}^{(1)}$ does not numerically depend on the strength of basic flow, the way the terms appear (i.e., q and term proportional to Ma) in the expression of $c_{\text{RP}}^{(1)}$ (or imaginary part of eigenvalue) does depend on whether the basic flow is present or not.

C. The stationary film ($\text{Bo} = 0$) case

To show this difference in the way of appearance of terms (particularly, terms proportional to Ma) in eigenvalues corresponding to $\text{Bo} = 0$ and $\text{Bo} \neq 0$ cases, we carried out an independent low- k analysis for a stationary liquid film (i.e., with $\bar{v}_z = 0$ or $\text{Bo} = 0$). This analysis also shows that the surfactant is unable to completely stabilize the RP instability in absence of flow. The leading-order velocity field is zero in absence of flow [refer to Eq. (24)], and hence, the leading-order kinematic condition Eq. (22c) gives $c_{\text{RP}}^{(0)} = 0$. Similarly, it is evident that $c_{\text{Ma}}^{(0)} = 0$ using surfactant transport equation [Eq. (22d)]. The equations at $O(k)$ are solved for first correction to wave speed using $c^{(0)} = 0$ and $\bar{v}_z = 0$. The eigenvalue correct up to $O(k)$ for zero flow case is given as

$$c_{@Bo=0} = \frac{ik}{2} \{ (q - \text{Ma}q_1) \pm \sqrt{[(q - \text{Ma}q_1)^2 + \text{Ma}q_2]} \}, \quad (34)$$

where q , q_1 , and q_2 are positive functions of S (refer to Appendix B). When $\text{Ma} = 0$, the above expression with negative sign becomes zero, and hence, the above expression with positive sign before the square root term captures the RP capillary instability of a clean stationary film. This also implies that the expression with plus sign corresponds to the RP mode, and the expression with negative sign corresponds to

the Marangoni mode. Since q , q_1 , and q_2 all remain positive, the above expression shows that the root with plus sign, i.e., RP mode, will never become stable on increasing Marangoni number. However, the Marangoni mode (root with negative sign) always remains stable. A comparison of Eqs. (33) and (34) shows that the way the terms appear in RP mode eigenvalue for $Bo = 0$ prevents it to become stable for any value of Ma in contrast to the case of $Bo \neq 0$ where the RP instability is suppressed above a critical Marangoni number.

The discussion given above in context of RP mode captured by Eq. (34) for $Bo = 0$ and Eq. (33) for $Bo \neq 0$ demands some more attention as explained in the following. The zero Bond number case predicts instability irrespective of the value of Marangoni number while the nonzero Bond number case predicts instability suppression above a critical Marangoni number Ma_{crit} , and this Ma_{crit} is found to remain independent of Bond number. This independence of Ma_{crit} with respect to Bond number lead us to infer that the instability suppression holds even when Bond number is infinitesimally small. However, it is expected that the film must remain unstable for the case of infinitesimally small Bond number as depicted by the case of Bond number being identically zero. A possible reason for such disagreement between zero Bond number case with infinitesimally small Bond number case could be appearance of ratio of Bond number to wave number in the analysis. If we carefully look at the details of long-wave analysis, then this ratio of Bo/k does play an important role in retaining or neglecting terms at leading order and/or first correction while performing the analysis. As an example, the tangential stress balance at gas-liquid interface is: $ik\tilde{v}_r + d_r\tilde{v}_z + \tilde{h}(d_r^2\tilde{v}_z) + ikMa\tilde{\Gamma} = 0$ with $\tilde{v}_r \sim O(1)$, $\tilde{v}_z \sim O(1/k)$, $\tilde{h} \sim O(1/k)$ (for low-wave-number analysis), and $d_r^2\tilde{v}_z|_{r=+1} = -Bo$. On substitution of all the variables in a series of k according to the respective scaling of each variable, the tangential stress balance can be written as

$$ik(\tilde{v}_r^{(0)} + k\tilde{v}_r^{(1)}) + \frac{1}{k}(d_r\tilde{v}_z^{(0)} + kd_r\tilde{v}_z^{(1)}) + \frac{1}{k}(\tilde{h}^{(0)} + k\tilde{h}^{(1)})(-Bo) + iMa(\tilde{\Gamma}^{(0)} + k\tilde{\Gamma}^{(1)}) = 0. \quad (35)$$

The leading-order tangential stress balance is obtained by collecting terms of $O(1/k)$ from above equation. The leading-order contribution of the term $\tilde{h}(d_r^2\tilde{v}_z)$ will come from expression $\frac{1}{k}\tilde{h}^{(0)}(-Bo)$. This contribution will remain $O(1/k)$ quantity only when Bond number is finite and $O(1)$. It has already been mentioned at the start of Sec. IV that Bond number is assumed to be an $O(1)$ quantity. When $Bo \rightarrow 0$ and $k \rightarrow 0$, we cannot conclude that the above mentioned contribution will remain an $O(1/k)$ quantity so as to be included in leading-order tangential stress balance. Equation (33) is obtained by considering Bond number to be an $O(1)$ quantity, and by retaining the above leading-order contribution at $O(1/k)$ in tangential stress balance. Thus, the prediction regarding instability suppression using Eq. (33) will be strictly valid only when Bond number remains an $O(1)$ quantity. Further, the above arguments put question on the validity of range of small wave numbers (numerically) up to which Eq. (33) holds. This is because one can always choose small

enough wave numbers and a small Bond number such that the $O(1/k)$ term at leading order from $\frac{1}{k}\tilde{h}^{(0)}(-Bo)$ may not be unimportant in the analysis. An idea about the validity of range of wave numbers up to which the Ma_{crit} value for instability suppression holds can be obtained by numerical continuation of Marangoni number values from sufficiently small wave number to finite and arbitrary wave numbers at small values of Bond number. We discuss this aspect in more detail when we present neutral stability curves in Marangoni versus wave number plane in the later part of this work.

V. RESULTS AT ARBITRARY WAVE NUMBER

Before we present results, it is useful to discuss the choice of different dimensionless parameters, and a possible estimate of dimensional parameters for which the results presented would be expected to hold in practice. As mentioned in Sec. II, there are three dimensionless parameters that appear in equations governing the stability of film flow [refer to Eq. (4)]. Further, we have assumed creeping flow limit which implies that the Reynolds number is zero. The Reynolds number, if inertial terms were taken into account, would be equal to $Re = \frac{\rho\gamma_0 h_0}{\mu^2}$. The air-liquid interfacial tension for several viscous liquid is $\gamma_0 \sim 0.01$ N/m, and if we set $\rho \sim 10^3$ kg/m³; the Reynolds number will be estimated as $Re \sim 10^{-2}h_0/\mu^2$, where h_0 is the film thickness in mm, and μ is the viscosity in Pa s. Thus, $Re \lesssim 0.01$ for $\mu \gtrsim 1$ Pa s and $h_0 \sim 1$ mm, or equivalently, the creeping flow approximation will hold only for viscous liquid films. Note that a decrease in h_0 from 1 mm will further reduce the Reynolds number. The Marangoni number varies between 0.01 for low surfactant concentration to ~ 1 for moderate concentrations [19]. The other two important parameters are: (i) Bond number ($Bo = \rho gh_0^2/\gamma_0$) which signifies the strength of basic flow, and (ii) the relative ratio of fiber or rod radius to film thickness ($S = R_0/h_0$). For $\rho \sim 10^3$ kg/m³, $g \approx 10$ m/s², and $\gamma_0 \sim 0.01$ N/m, the Bond number is estimated as $Bo \sim h_0^2$, where h_0 is the film thickness in mm. All the results are presented by fixing Bo and varying S and/or Marangoni number. Assigning a value to Bond number implies that the film thickness is fixed, and for fixed h_0 , variation in S means a change of rod/fiber radius relative to a given film thickness. The values of Bo and $S(= R_0/h_0)$ are selected in such a manner that both h_0 and R_0 remain in the between 0.1 and 1 mm.

A. Growth-rate versus wave-number results

The low-wave-number results presented above demonstrated that the RP instability can be suppressed when Marangoni number increases above a critical value while the surfactant mode always remains stable in low- k limit. In this section, we continue the eigenvalues obtained above for RP mode [Eq. (33)] and surfactant mode [Eq. (32)] from low wave numbers to finite and arbitrary wave numbers. Recall that this is equivalent to continuing the two roots (root-1 and root-2) of the quadratic characteristic equation as per the discussion given in Sec. III. The results are presented in the form of growth-rate versus wave-number data and neutral stability curves in Ma versus wave-number plane. Following previous studies related to cylindrical film flows, we rescale wave number using unperturbed GL interface location

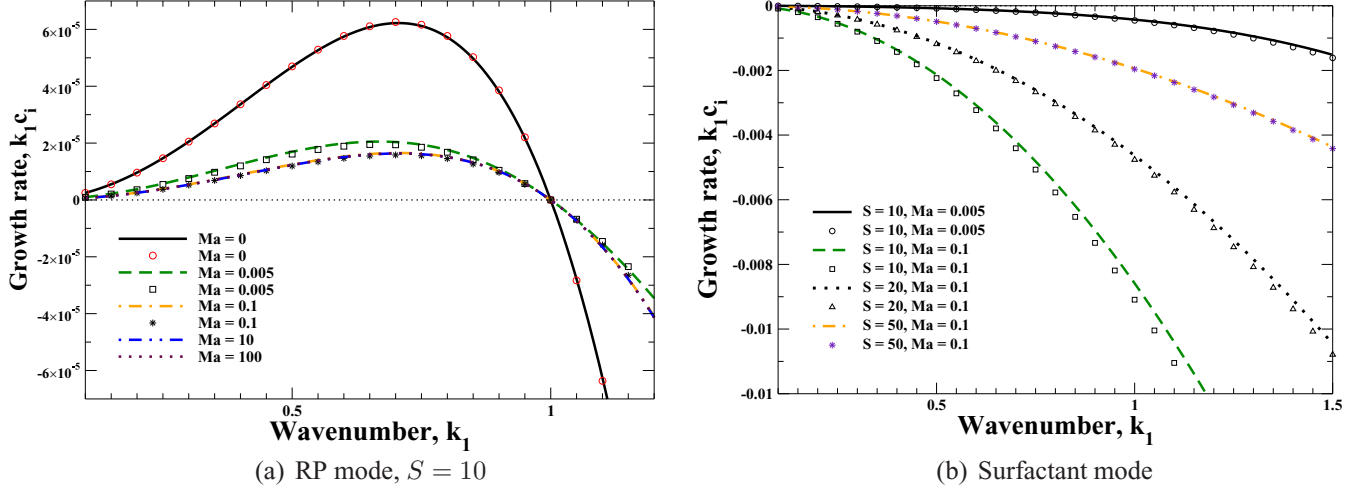


FIG. 2. Growth-rate vs. wave-number data for a stationary film ($Bo = 0$). The continuous lines (solid, dashed, dash-dotted, etc.) correspond to present results while symbols (open circle, open square, star, etc.) represent data points obtained using Carroll and Lucassen's growth-rate Eq. (37).

(i.e., $R_0 + h_0$) instead of film thickness (h_0) to present the results. The rescaled wave number is denoted as k_1 and is related to k as $k_1 = k(S + 1)$. It is well known for cylindrical liquid threads or films that the growth-rate for RP instability goes from positive to negative when the dimensional wave number is equal to the inverse of (unperturbed) gas-liquid interfacial location measured from the central axis (for example, refer reviews by Eggers and Villermaux [39], and Gallaire and Brun [40]). The growth-rate (GR) of RP instability for clean cylindrical liquid film, in fact, scales with k_1 as $GR \sim k_1^2 (1 - k_1^2)$. A similar scaling is also observed for surfactant-laden stationary film ($Bo = 0$) coating over a cylindrical rod [23]. Thus, $k_1 = 1$ represents the cutoff wave number where the growth-rate switches from positive to negative values in these earlier studies. This is precisely the reason that we rescaled wave number using $(R_0 + h_0)$ while presenting results.

Figures 2(a) and 2(b) show the growth-rate versus wave-number data for RP and surfactant mode, respectively, for a stationary film ($Bo = 0$). These two figures also provide a comparison of results obtained here with Carroll and Lucassen's work [23] who examined the stability of surfactant-laden liquid film coating over a fiber in the limit of zero Bond number. They derived the equation governing the growth-rate (denoted as β^* in their paper) using thin film approximation, and the nondimensional form of their equation for growth-rate using present scheme of nondimensionalization is

$$\beta = \left[\frac{(1 - k_1^2)k_1^2}{12(S + 1)^3} \right] \left[\frac{4\beta(S + 1)^2 + Ma k_1^2}{\beta(S + 1)^2 + Ma k_1^2} \right]. \quad (36)$$

The two roots of the above equation are

$$\beta = \frac{k_1^2}{6(S + 1)^3} \left[B_1 \pm \sqrt{B_1^2 + 3Ma(S + 1)^2(1 - k_1^2)} \right], \quad (37)$$

where, $B_1 = 1 - k_1^2 - 3Ma(S + 1)^2$. Since, the scaling used to write down above equation is consistent with the current scheme of nondimensionalization, β is same as $k_1 c_i$. Follow-

ing the procedure outlined in context of Eq. (34), the root with positive sign before square-root term captures the Rayleigh-Plateau instability, and the root with negative sign before square-root term corresponds to surfactant/Marangoni mode. The different symbols (open circle, square, star, etc.) in Fig. 2 correspond to Carroll and Lucassen's result using Eq. (37), and continuous lines (solid, dashed, dash-dotted, etc.) represent data obtained in the present work. Figures 2(a) and 2(b) show a good agreement between our results and previous results [23] for both RP and surfactant modes. Note that the data in Fig. 2(b) shows that the agreement between our results and previous results get better with increase in value of S . This is expected because Carroll and Lucassen's analysis is valid in the limit of thin film as compared to rod radius. An increase in S implies a decrease in film thickness h_0 with respect to rod radius R_0 , thus, we observe a better match at higher values of S . Figure 2(a) clearly shows that the growth-rate of RP instability is reduced as Marangoni number becomes nonzero. We have verified that the growth-rate reduces approximately by a factor of 4 with sufficient increase in Marangoni number, but the RP instability is never completely suppressed. This observation is also in agreement with previous studies related to the effect of surfactant on the RP instability of stationary ($Bo = 0$) cylindrical films [19,23]. While the data in Fig. 2(a) is shown for $S = 10$, we have verified that the RP mode does not become stable for other values of S for $Bo = 0$. We have also verified that the surfactant mode always remains stable for different values of S and Ma for $Bo = 0$ [for example, as shown in Fig. 2(b)].

Figure 3 shows the growth-rate versus wave-number data for RP mode and surfactant mode in presence of flow ($Bo = 0.25$) at $S = 1$. Figure 3(a) shows that the clean film ($Ma = 0$) remains unstable owing to the presence of Rayleigh-Plateau instability. With increase in Marangoni number, the growth rates as well as the band of unstable wave numbers decrease, and the RP instability is completely suppressed above a particular value of Marangoni number. The growth-rates are observed to be negative for $Ma = 0.2$ in Fig. 3(a), and further increase in Ma results in increased decay rates. In

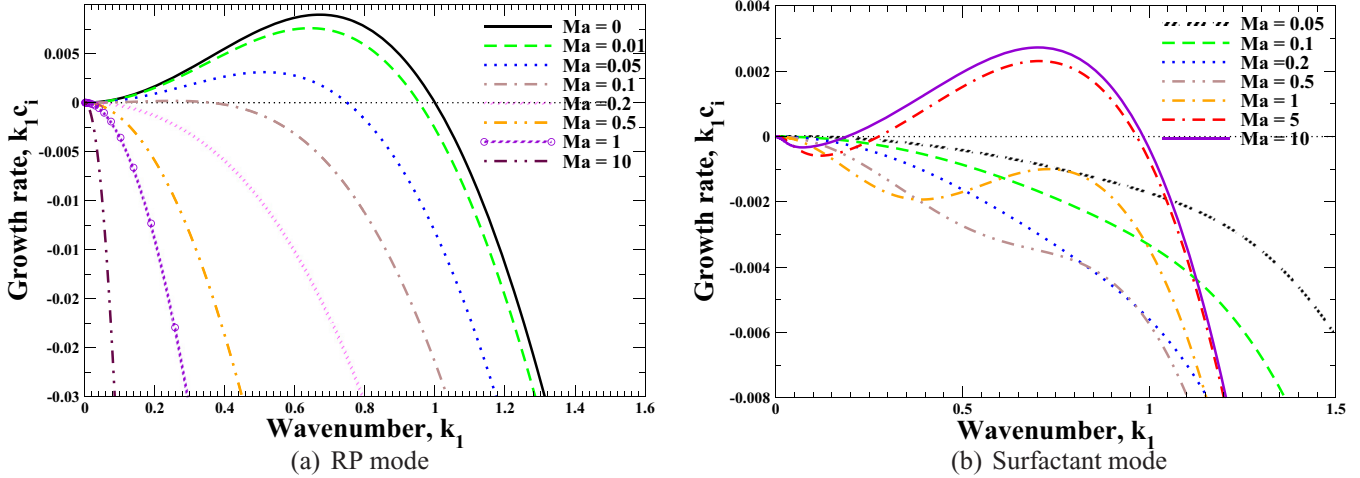


FIG. 3. Growth-rate vs. wave-number data for $Bo = 0.25$, and $S = 1$.

contrast, the surfactant mode perturbations remain stable at small Marangoni numbers, however, become unstable when Ma is sufficiently increased. For example, Fig. 3(b) shows that the surfactant mode remains stable for $Ma = 0.05$ and the decay rate increases with increase in Ma up to 0.2. However, for $Ma = 0.5$, there is a slight decrease in the decay rate of surfactant mode in the vicinity of $k \lesssim 1$. This decrease in decay rate with increase in Marangoni number is more clearly evident at $Ma = 1$, and finally, positive growth rates are observed for surfactant mode at $Ma = 5$ and 10. Thus, while RP instability is suppressed on increasing the Marangoni number, the surfactant mode becomes unstable when Ma is sufficiently increased. However, there is a range of Marangoni numbers where the RP instability is suppressed without triggering the surfactant mode instability. For example, in Fig. 3, both the modes are observed to remain stable between $Ma = 0.2$ and $Ma \sim 1$.

Figure 4 shows the growth-rate versus wave-number data for a smaller value of Bo ($= 0.04$) at two different values of S . Figure 4(a) shows that the RP mode remains unstable for $Ma = 0$ and increasing Marangoni number has a stabilizing effect on RP instability in a manner similar to shown in Fig. 3(a). This figure shows that the RP mode becomes stable for $Ma \geq 0.2$. The surfactant mode which remains stable at small enough values of Marangoni number become unstable with increase in Marangoni number [refer to Fig. 4(b)]. However, Figs. 4(a) and 4(b) show that while RP instability exists at $Ma = 0.1$ and is suppressed for $Ma \geq 0.2$, the surfactant mode becomes unstable at $Ma = 0.1$ and remains unstable on further increase of Marangoni number. Thus, the RP instability is still suppressed by increase of Marangoni number but the surfactant mode instability triggers in at sufficiently low Marangoni numbers to render the film flow unstable. These figures [Figs. 4(a) and 4(b)] suggest that a stability window in terms of Marangoni number does not exist for $Bo = 0.04$, $S = 1$ while a stable gap in terms of Ma was possible for $Bo = 0.25$, $S = 1$ (Fig. 3). Further, when S is increased from 1 to 2.5, Figs. 4(c) and 4(d) demonstrate that it is possible to obtain stable film flow configuration by selecting an appropriate value of Marangoni number. Recall that the surface tension has a destabilizing effect on RP instability arising due to

circumferential curvature $[1/(S + 1)]$ of GL interface. With increase in S , the circumferential curvature decreases which results in reduced destabilizing effect of surface tension on RP mode for $S = 2.5$ as compared to $S = 1$. Thus, the RP instability is suppressed at low Marangoni numbers at $S = 2.5$ as compared to $S = 1$. This can be observed by analyzing growth-rate versus wave-number data for RP mode given in Fig. 4(a) for $S = 1$ and Fig. 4(c) for $S = 2.5$. Figure 4(c) shows that the RP mode instability is suppressed at $Ma = 0.05$ for $S = 2.5$ while the RP mode remains unstable up to $Ma = 0.1$ for $S = 1$ as shown in Fig. 4(a). In a similar manner, one can observe using Figs. 4(b) and 4(d) that the effect of increasing S is stabilizing for surfactant mode as well. Since the effect of increasing S is stabilizing for both RP and surfactant modes, it is possible to obtain stable film flow configuration when S is increased from 1 to 2.5. These data in Figs. 3 and 4 suggest that the possibility of obtaining a stable film flow configuration depends on the values of Bo and S . To get a clear idea about the parameter ranges where a surfactant could be used to obtain stable film flows, we next show neutral stability curves in Ma - k_1 plane which demarcates stable and unstable region for given Bond number and S .

B. Neutral stability curves

Before we present the neutral curves for nonzero Bond numbers, we refer to Fig. 2 to get an idea about the neutral curves at $Bo = 0$. Figure 2 shows that the presence of surfactant is not able to completely suppress the RP instability and the RP mode remains unstable from $k_1 \rightarrow 0$ to $k_1 = 1$. However, the surfactant mode is never observed to become unstable for any wave number. Thus, only one neutral curve corresponding to RP mode will exist for $Bo = 0$. The growth-rate versus wave-number data for RP mode in Fig. 2(a) shows that the growth-rate changes sign from positive to negative at $k_1 = 1$ irrespective of the value of Marangoni number. Even though the data in Fig. 2(a) is shown for $S = 10$, we have verified that the cutoff wave number remains 1 irrespective of the values of S and Ma . Thus, the neutral curve for RP mode in Ma versus k_1 plane will simply be a vertical straight line $k_1 = 1$ with region left to this line (i.e., $k_1 < 1$) being unstable

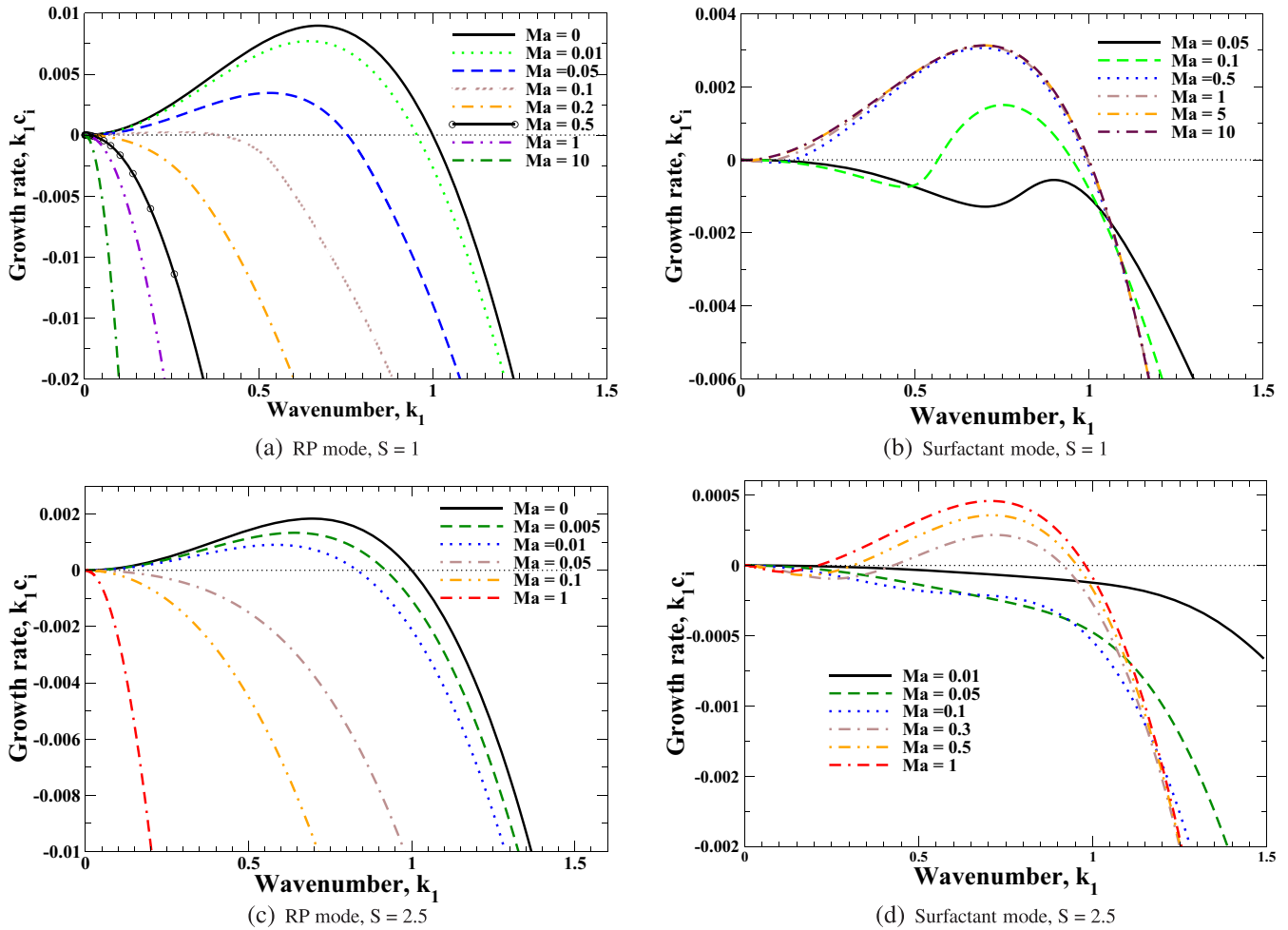


FIG. 4. Growth-rate vs. wave-number data for $Bo = 0.04$.

region while the right side of the line ($k_1 > 1$) is the stable region. We next focus our attention on neutral stability data for nonzero Bond numbers.

Typically, two neutral curves exist for a given value of Bo and S : a lower neutral curve corresponding to RP mode and an upper curve corresponding to surfactant mode. Figure 5(a) shows neutral stability curves for $Bo = 0.25$ and at different values of S . Let us first focus on a particular value of S , say $S = 2$. The RP mode is unstable for $Ma = 0$ and at small values of Marangoni number. However, the surfactant mode remains stable at sufficiently lower values of Marangoni number. As Marangoni number increases above the lower neutral curve, the perturbations corresponding to RP mode are suppressed. With further increase in Marangoni number, we encounter an upper neutral curve which corresponds to the destabilization of surfactant mode [as shown in Figs. 3(a), 4(b) and 4(d)]. Figure 5(a) shows that the critical value of Marangoni number above which RP instability gets suppressed is $Ma \approx 0.45$, and the Marangoni number above which surfactant mode becomes unstable is $Ma \approx 4.1$. Thus, for $S = 2$ and $Bo = 0.25$, there exists a wide gap in between the lower RP mode neutral curve and upper surfactant mode neutral curve where both the modes remain stable. This implies that the film flow configuration which was otherwise unstable due to RP instability in the clean film

limit ($Ma \rightarrow 0$) can be made stable by appropriately selecting the value of Marangoni number, or equivalently, by choosing the sufficient concentration of an interfacial surfactant. Note that the threshold value of Ma above which the suppression of RP instability is achieved is determined by long-wave perturbations, and hence, the critical value for lower neutral curve can always be evaluated using long-wave results, i.e., Eq. (33). Figure 5(a) shows that with decrease in value of S from 2, the lower neutral curve moves up and the upper curve shifts down thereby decreasing the stable gap where both the modes remain stable. This figure shows that the stability window almost vanishes when S is decreased to 0.2.

Figure 5(b) shows the neutral stability diagram for $Bo = 0.04$ and at different values of S . This figure demonstrates that a stable gap exists between lower and upper neutral curves for $S = 5$ and 2.5, however, the gap disappears when S decreases to 1 and 0.5. Figure 5(b) shows that the upper and lower neutral curves continue to exist as two separate curves for $S = 5, 2.5$, and 1. However, for $S = 0.5$, both the upper and lower neutral curves split into two branches with left branch of upper curve merging with left branch of lower neutral curve (toward low- k_1 side), and right branch of upper curve joining with right branch of lower neutral curve (near to $k_1 \approx 1$). Figure 6(a) shows the neutral curves for $Bo = 0.01$ and different values of S . This figure also depicts that the

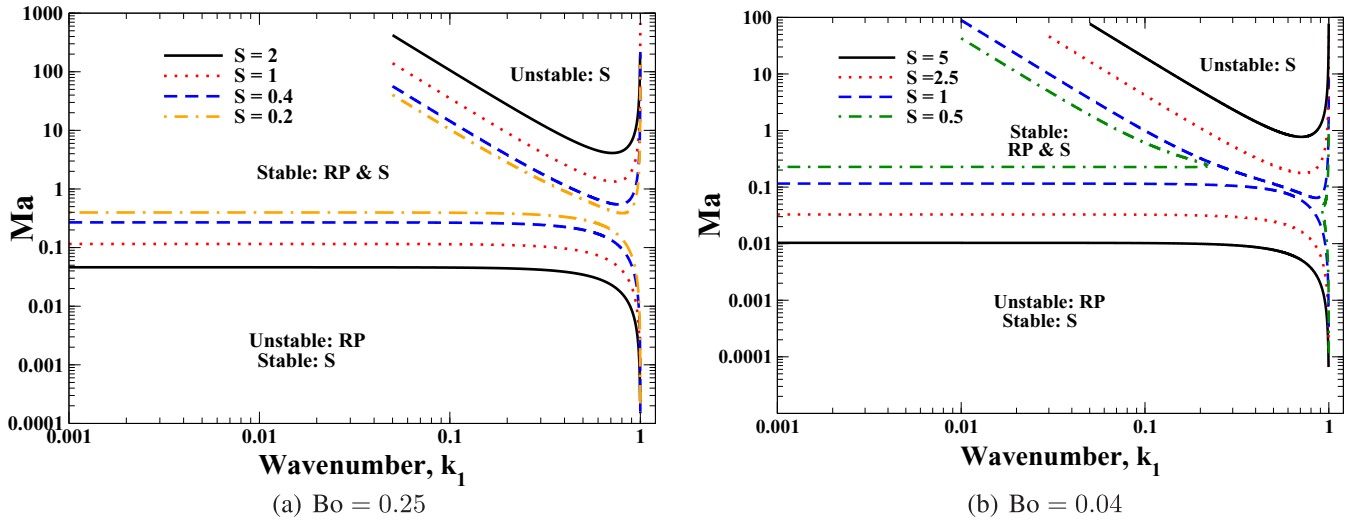


FIG. 5. Neutral stability diagram in Ma vs. k_1 plane. “S” denotes surfactant mode.

stable gap is present at higher values of S , and this gap decreases with decrease in S and finally disappears for low enough values of S . Figure 6(a) shows the merging of neutral curves corresponding to the two roots (identified as RP mode and surfactant mode) for $S = 1$, and $Bo = 0.01$ in a manner similar to as shown in Fig. 5(a) for $S = 0.5$ and $Bo = 0.04$. In contrast to the above mentioned figures [Figs. 5 and 6(a)], a stability window in terms of Ma is always present for $Bo = 1$ as shown in Fig. 6(b). The RP instability is suppressed for a wide range of Marangoni numbers without triggering the surfactant mode instability for all the values of S reported in Fig. 6(b). Of course, the width of stable gap decreases with decrease in value of S in agreement with the neutral stability results presented for other (smaller) values of Bond number.

It is useful to look at the above results in terms of dimensional values of film thickness and fiber radius. To do that, we set $\rho = 10^3 \text{ kg/m}^3$, $g \approx 10 \text{ m/s}^2$, $\mu = 1 \text{ Pa s}$, and $\gamma_0 \sim 0.01 \text{ N/m}$. This is equivalent to considering a particular liquid, and substituting them in the expression of Bond num-

ber gives $Bo = h_0^2$ as mentioned at the start of this section. Thus, $h_0 = 0.5, 0.2, 0.1$, and 1 mm , respectively, when $Bo = 0.25, 0.04, 0.01$, and 1 in Figs. 5 and 6. The fiber radius can then be calculated using $S = R_0/h_0$. Hence, a decrease in S for a given Bo implies a reduction in fiber radius for a given liquid film thickness. We have varied S in such a manner that the largest value of S in a given neutral stability diagram (i.e., for a given Bo) corresponds to 1-mm-thick film, and the smallest S gives $R_0 = 0.1 \text{ mm}$. Thus, all the figures depicting neutral curves above show that the effect of decreasing the fiber radius for a fixed h_0 is destabilizing for the surfactant-laden liquid film flow configuration considered in the present work. For example, the film thickness is 0.1 mm in Fig. 6(a) and $S = 10$ gives $R_0 = 1 \text{ mm}$. A wide stable gap is present for this parameter set where RP instability is suppressed without activating the surfactant mode instability, and thus, the clean film configuration which remains unstable due to RP instability can be made stable by using an interfacial surfactant. However, when $S = 3$ or 1 (i.e., $R_0 = 0.3$ or 0.1 mm , respectively, and h_0 is still 0.1 mm), the stable gap

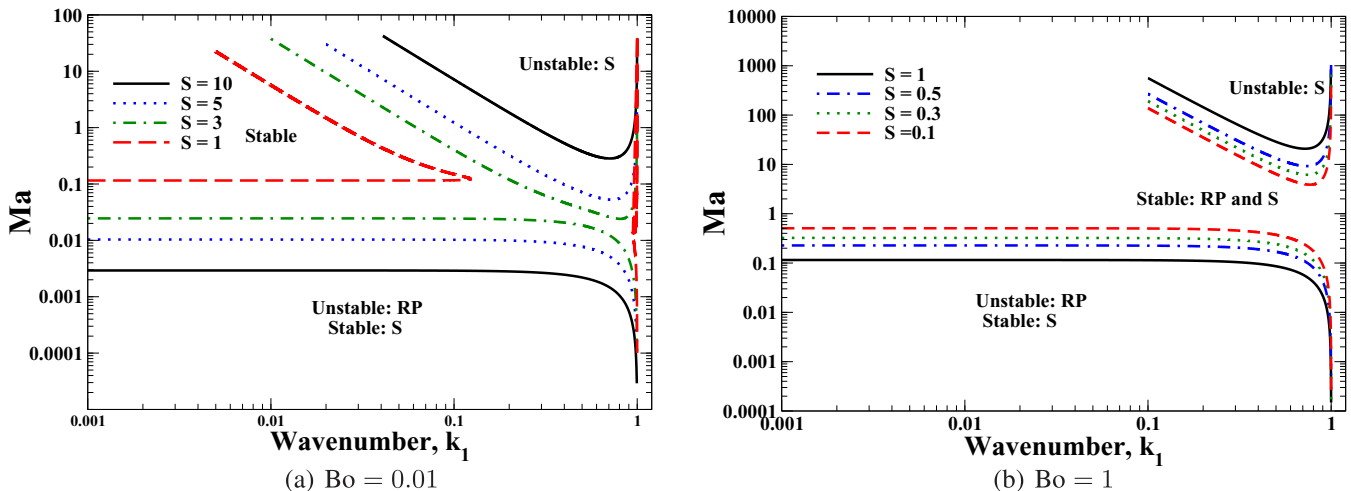


FIG. 6. Neutral stability diagram in Ma vs. k_1 plane.

almost vanishes or remains absent because of merging of upper and lower neutral curves (for $S = 1$). Thus, thinning the fiber for a given film thickness is destabilizing for the system under investigation. While this observation holds, we also observe that the film flow remains most stable at $Bo = 1$ followed by $Bo = 0.25$ case. We anticipate this increased stability of film flow at higher Bond numbers to be related to the strength of basic flow. We can get an idea about the strength of base flow by evaluating the expression $\bar{v}_z(r)$, i.e., Eq. (16), at GL interface (at $r = S + 1$). We have verified that the function $f(r)_{@r=S+1}$ in Eq. (16) is a monotonic decreasing function of S , and is close to 4.1 at $S = 0.1$ while it remains below 2 as S increases to very high value. In fact $f(S + 1) \rightarrow 2$ as $S \rightarrow \infty$. Thus, $f(S + 1)$ remains an $O(1)$ number and the order of magnitude of base flow at GL interface is decided by Bond number. For example, we have verified using Eq. (16) that the nondimensional basic free-surface velocity remains approximately between 0.005–0.006 for $Bo = 0.01$ for the values of S used in Fig. 6(a). The $\bar{v}_{z@r=S+1}$ increases significantly and lies between 0.6–1.1 for $Bo = 1$ and at different S used in Fig. 6(b). These observations confirm that the magnitude of Bond number determines the strength of base flow as compared to $f(r)$ appearing in expression of Eq. (16). Hence, we infer that the existence of more stable film flow configuration at high Bond number is a result of increased strength of base flow.

Another point worth noting from neutral stability diagrams is that the surfactant mode becomes unstable even at low wave numbers for high enough values of Marangoni number. This feature is more evident if we focus on the neutral curve corresponding to surfactant mode for $Bo = 0.01$ and $S = 1$ in Fig. 6(a) or for $Bo = 0.04$ and $S = 0.5$ in Fig. 5(b). For all other surfactant mode neutral curves in Figs. 5 and 6 as well, the upper curve continues to low wave numbers. In contradiction to this observation, the low- k eigenvalue expression for surfactant mode [Eq. (32)] found in Section IV predicted that the surfactant mode will never become unstable on increasing the value of Marangoni number. However, the low- k analysis presented in Sec. IV assumed $Ma \sim O(1)$ which implies that the Marangoni number does not scale with wave number in any manner and remains independent of wave number. However, the neutral curves for surfactant mode in above figures clearly show that the critical Marangoni number scales with wave number in a particular fashion. We examined the neutral stability data and found that critical Ma increases as $1/k^2$ for $k \ll 1$. We then performed a low-wave-number analysis considering the scaling $Ma \sim 1/k^2$ to capture the surfactant mode neutral curve in $k \ll 1$ limit. This analysis remains similar to the low-wave-number analysis presented in Section IV with modifications in conditions at GL interface because of scaling of Ma with wave number. The details of the asymptotic analysis are presented in Appendix A. The expression of critical Marangoni number obtained from this analysis is

$$Ma_{\text{crit}} = \frac{Bo^2}{64k^2} \frac{g_1}{(1+S)^6 q_1^2}, \quad (38)$$

where g_1 is a positive valued function of S given in Appendix B. The functions q_1 (also a positive valued function)

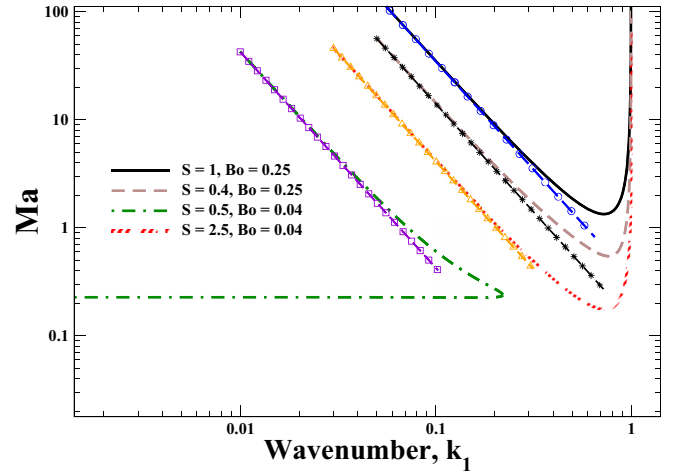


FIG. 7. Comparison of surfactant mode neutral curve branch in low-wave-number limit with asymptotic result. The dashed lines with symbols (open circle, star, open square, and open triangle) represent the Marangoni number evaluated using Eq. (38).

was defined earlier and is also given in Appendix B. Figure 7 compares the neutral curve data with the value of critical Marangoni number evaluated using Eq. (38). Note that k is rescaled to k_1 as done earlier to present results at arbitrary wave numbers. This figure clearly shows an excellent match between the Ma obtained from asymptotic results with Ma values depicted in upper neutral curves in low- k limit. It is worth to recall here that, in practice, the Marangoni number varies between $O(10^{-2})$ to $O(1)$. The upper neutral curves in Fig. 7 (as well as in Figs. 5 and 6) are extrapolated to very high values of Marangoni number (~ 10 or 100) and the data at such large Ma values is not of any practical interest. However, the values of Ma which really are important in practice are the threshold value above which the RP instability is suppressed, and the minimum of upper neutral curve above which the surfactant mode instability is triggered. The neutral curves shown in in Figs. 5 and 6 clearly show that these two values fall in range of $O(10^{-2})$ – $O(1)$ which are practically feasible.

At this point, it is important to recall the issue raised at the end of Section IV. The surfactant-laden film is known to remain unstable in absence of flow ($Bo = 0$). Specifically, the RP mode remains unstable for perturbations with infinitesimally small wave numbers ($k_1 \rightarrow 0$) to $k_1 = 1$ at $Bo = 0$. Therefore, it is expected that the surfactant-laden film flow configuration will remain unstable in the limit of infinitesimally small Bond number. It was argued at the end of Sec. IV that the prediction of RP instability suppression in low-wave-number limit using Eq. (33) is strictly valid only when Bond number is an $O(1)$ quantity. It was also mentioned that the range of (small) wave numbers up to which Eq. (33) holds may get affected at smaller values of Bond number. This effect of decreasing Bond number toward smaller values can be seen by constructing lower neutral curves starting from very low wave numbers (i.e., say $k_1 = 0.001$ or lower, where $Ma_{\text{crit}} = q/n$ is expected to hold true) and continuing them numerically to finite and arbitrary wave numbers. However, before we present neutral curves at different (small) Bond numbers, it is useful to look at the eigenvalue expression eval-

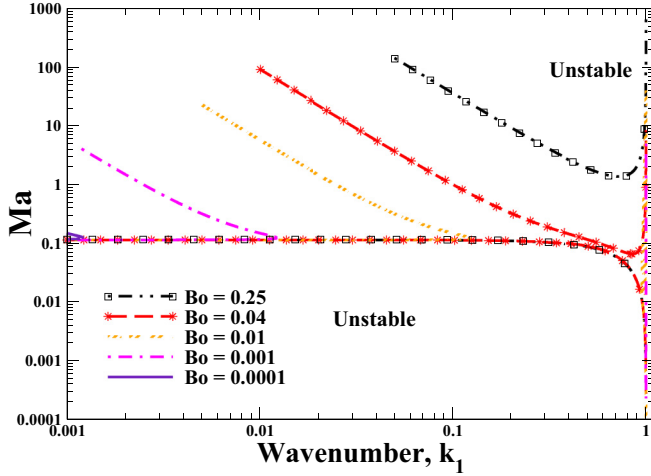


FIG. 8. Neutral stability curves at $S = 1$ and with varying Bond number.

uated in Appendix A in the limit of long-wave disturbances and $Ma \sim 1/k^2$. The eigenvalue obtained from the analysis can be written as

$$c = c^{(0)} + kc^{(1)} = Bo\zeta_1 + ik \frac{q_2}{q_1} \left[1 - \frac{Bo^2}{64M} \frac{g_1}{(1+S)^6 q_1^2} \right]. \quad (39)$$

Here, ζ_1 and q_2 are positive valued function of S (given in Appendix B). The eigenvalue expression given above shows that the growth-rate depends on Bond number. The expression in Eq. (39) reduces to $c = \frac{ikq_2}{4q_1}$ for $Bo = 0$. The eigenvalue in the limit of long-wave disturbances at $Bo = 0$ is earlier reported in Sec. IV in Eq. (34). Recall that the expression with positive sign before square root term in Eq. (34) corresponds to RP mode; and it can be shown that this RP mode eigenvalue in Eq. (34) reduces to $\frac{ikq_2}{4q_1}$ in the limit of very high Marangoni number. This implies that the expression of c [Eq. (39)] obtained from the low-wave-number analysis presented in Appendix A with $Ma \sim 1/k^2 \gg 1$ captures the RP mode instability in the limit of zero basic flow ($Bo = 0$). Thus, at $Bo = 0$, Eq. (39) predicts instability with growth-rate identically equal to the zero flow growth-rate evaluated using Eq. (34) in the limit of high Marangoni number. Equation (39) further shows that increasing Bond number has a stabilizing effect on this positive growth-rate ($\frac{ikq_2}{4q_1}$) at fixed value of scaled Marangoni number M . This equation shows that there will be a transition from unstable to stable perturbations with increase in Bond number at a given value of M . Since, Eq. (39) captures the stabilizing effect of increasing flow strength (Bo) and is also finally used to evaluate the low- k branch of upper neutral curves; we expect that the effect of Bond number on upper neutral curves (as well as on lower neutral curves) could provide more insights in connecting results at zero Bond number and infinitesimally small Bond number.

As mentioned above, we have plotted neutral curves for a given S and examined how the stable and unstable regions vary as we systematically decrease the Bond number. Figure 8 shows the neutral stability diagram at $S = 1$ and for different values of Bond number. The figure clearly shows that a stable

gap exists at sufficiently high Bond number ($Bo = 0.25$), and as Bond number decreases to 0.04, the upper neutral curve shifts downwards so as to close the stable gap. The lower and upper neutral curves still exist as two distinct curves at $Bo = 0.04$. However, as Bond number is further decreased (to 0.01 and lower), both the upper and lower neutral curves split into two branches: left and right branch. The left (right) branch of upper curve merges with left (right) branch of lower neutral curve. The gap between the left and right merged branches is the unstable region. An important point to note is that the left merged branch keep shifting toward low wave numbers with decrease in Bond number while right branch remains a vertical line at $k_1 = 1$. This implies that the band of unstable region keeps shifting toward low wave numbers, and as $Bo \rightarrow 0$, the perturbations from $k_1 \rightarrow 0$ to $k_1 = 1$ remains unstable. This figure also provides information about the range of validity of small wave numbers up to which Eq. (33) (or equivalently, $Ma_{\text{crit}} = q/n$) will hold true. For $S = 1$, the critical Marangoni predicted from low-wave-number expression is $Ma_{\text{crit}} = q/n = 0.115$. The lower neutral curves in Fig. 8 clearly show that the range of wave numbers up to which this long-wave threshold Marangoni number continues decreases with decrease in Bond number. For example, the critical value of Marangoni number Ma_{crit} holds up to $k_1 \approx 0.1$ for $Bo = 0.01$. This range decreases to $k_1 \lesssim 0.01$ and $k_1 \lesssim 0.001$ for $Bo = 10^{-3}$ and 10^{-4} , respectively. Thus, as Bond number becomes infinitesimally small, the wave number up to which Ma_{crit} value is valid (for transition from unstable to stable perturbations) also becomes infinitesimally small. This implies that there always exists (theoretically) an infinitesimally small wave number for infinitesimally small Bond number up to which Eq. (33) holds, however, for all practical purposes, the film flow configuration remains unstable in the limit of infinitesimally small Bond numbers which is in agreement with the results corresponding to $Bo = 0$.

We now focus on one major difference in finding out the wave speed using the analysis given in Appendix A with $Ma \sim 1/k^2$ as compared to the eigenvalue calculation for surfactant mode [with $Ma \sim O(1)$] given previously in Eq. (32) in Sec. IV. An important aspect that emerges out of the following discussion is that the instability captured by upper neutral curves does not belong to the true surfactant mode as per the definition given in earlier studies related to stability of surfactant-laden film flows [24,33,42–44]. The leading-order wave speed solution that exists purely because of presence of surfactant concentration fluctuation (i.e., $\tilde{\Gamma}^{(0)} \neq 0$) without necessarily having a perturbation in gas-liquid interface location (i.e., with $\tilde{h}^{(0)} = 0$) is identified as surfactant mode in low- k limit [24,33,42–44] (also refer discussion just preceding Eq. (29) in Sec. IV). Thus, the calculations given in Sec. IV used $\tilde{h}^{(0)} = 0$, and $\tilde{\Gamma}^{(0)} \neq 0$ to find out surfactant mode eigenvalue given in Eq. (32). In contrast, the analysis given in Appendix A with $Ma \sim 1/k^2$ requires both $\tilde{h}^{(0)}$ and $\tilde{\Gamma}^{(0)}$ to be nonzero to capture the (unstable) eigenvalues depicted by upper neutral curves in $k \ll 1$ limit. We have verified that the leading-order and first correction equations given in Appendix A gives a zero trivial solution if we consider $\tilde{h}^{(0)} = 0$, and $\tilde{\Gamma}^{(0)} \neq 0$ while incorporating the scaling $Ma \sim 1/k^2$. Since, the instability captured at higher Ma ($\sim 1/k^2$) requires the presence of fluc-

tuations in both surfactant concentration and GL interface location, this instability does not belong to the pure surfactant mode as defined in earlier studies [24,33,42–44]. Another difference that appears due to $\tilde{h}^{(0)} \neq 0$ is that the leading-order flow is nonzero in the analysis given in Appendix A as compared to the low- k analysis given in Sec. IV for surfactant mode where the leading-order flow was absent. The leading-order velocities are proportional to $\tilde{h}^{(0)}$ in both the analysis [for example, refer to Eq. (24) or Eq. (A5)], and hence, they are zero or nonzero according to whether $\tilde{h}^{(0)}$ is zero or nonzero, respectively.

This observation about upper neutral curves not belonging to true surfactant mode becomes more important in context of the observation that the eigenvalue calculated in Appendix A reduces to RP mode eigenvalue in low wave number and high Marangoni number limit. These two observations suggest that the mechanism that drives the instability predicted by upper neutral curve could be the same as the mechanism for RP instability with later being modified by the presence of surfactant. The exact role played by surfactant in presence of basic flow in exciting the instability at higher Marangoni number and suppressing the instability at lower Marangoni number is an issue worth considering as future investigation. In view of this preceding discussion, the labeling of the upper neutral curves as surfactant mode neutral curves is not entirely correct. Recall that the two roots are labeled as RP or surfactant mode based on the low-wave-number behavior when Marangoni number is either small or an $O(1)$ quantity (refer to Sec. III). It is only in this sense that we identify the two roots (nominally) as RP or surfactant modes. While classifying the two roots as RP or surfactant mode is more a matter of labeling the eigenmodes, the more important aspect uncovered here is that there are two eigenmodes possible for the present flow configuration, and these two eigenmodes can become stable/unstable depending on the value of S , Bo , and Ma . The neutral stability results show that it is possible to choose values of Bond number and S such that both the eigenmodes (roots) remain stable. Of course, the results also show that for a given Bond number and sufficiently small value of S , it is not possible to stabilize the film flow past a cylindrical rod using interfacial surfactant.

VI. CONCLUSIONS

We have performed a linear stability analysis for a liquid film flowing past a cylindrical rod when the gas-liquid interface is loaded with an interfacial surfactant. In creeping flow limit, the characteristic equation is quadratic and the two roots (or eigen-modes) can be stable/unstable depending on parameters: Bond number, ratio of rod radius to film thickness (S), and Marangoni number. The two roots are labeled as Rayleigh-Plateau mode (root-1) and surfactant mode (root-2) based on their behavior in low-wave-number limit. The Rayleigh-Plateau mode (or root-1) always remains unstable for a clean film ($Ma = 0$), and earlier work by Carroll and Lucassen [23] demonstrated that the presence of surfactant have a partial stabilizing effect on Rayleigh-Plateau mode, and it is not possible to achieve a completely stable film flow configuration even in the limit of very high Marangoni number. Recall that they considered a stationary liquid film,

and hence, the effect of basic flow was ignored in their work. In contrast, we show that inclusion of basic flow in stability analysis results in complete stabilization of eigen-mode corresponding to root-1 (labeled as Rayleigh-Plateau mode). The instability corresponding to root-1 completely disappears when Marangoni number increases above a finite threshold value. Interestingly, the second root of characteristic equation, nominally labeled as surfactant mode, becomes unstable with increase in Marangoni number above a critical value for a given Bond number and S . Thus, the overall stability of the system is governed by a competition in between the two eigen-modes. Specifically, the stability depends on whether the critical value of Ma required for stabilization of root-1 is sufficiently larger than the critical value of Marangoni number required to destabilize the eigen-mode corresponding to root-2? Our results show that there exists a stable gap in terms of Ma where both the modes remain stable. This stable gap is usually found to exist at higher values of S for a given Bond number. The width of stability window decreases with decrease in S and finally vanishes for sufficiently small values of S at a given Bond number. In terms of dimensional variables, the above statement implies that for a given liquid and film thickness, the effect of decreasing rod radius is destabilizing. Further, the effect of increasing the Bond number is found to have an overall stabilizing effect on the film flow configuration. We argued that this increase in stabilization with increasing Bond number is a consequence of increased strength of basic flow.

To summarize, we have shown that depending upon a given S and Bond number (which is equivalent to specifying film thickness and rod radius for a given fluid), the clean film flow which otherwise remains unstable can be stabilized by using an interfacial surfactant by choosing right amount of surface concentration (i.e., according to the stable gap in Ma). However, this stabilization is not possible for all values of film thickness and rod radius (or Bond number and S) as one of the eigen-mode among the two possible modes become unstable for a band of wave numbers. These results are important because a complete stabilization of surfactant-laden cylindrical film flows has not been observed thus far in existing literature. This happens because of neglecting the basic flow in stability analysis in previous works while our analysis incorporates a nonzero base flow in the stability analysis.

ACKNOWLEDGMENTS

The authors thank the referees for their insightful comments and suggestions which helped us to present the work in a more clear manner. Gaurav Sharma thanks the Science and Engineering Research Board (SERB), Government of India, for funding the work through project Grant No. CRG/2018/003532.

APPENDIX A: LOW-WAVE-NUMBER ANALYSIS WITH $Ma \sim 1/k^2$

The surfactant mode neutral curve data reveals that $c_r \sim O(1)$ in low- k limit. Thus, the wave speed is expanded as: $c = c^{(0)} + kc^{(1)} + \dots$. Similar to the analysis given in Sec. IV, we obtain $\tilde{v}_r \sim O(1)$, $\tilde{v}_z \sim O(1/k)$, $\tilde{p} \sim O(1/k^2)$, and $\tilde{h} \sim$

$O(1/k)$. Considering $\text{Ma} = M/k^2$, where M is a constant independent of k , we get $\tilde{\Gamma} \sim O(1)$ from tangential/normal stress balance [Eq. (11) or (12)]. Since the scalings of \tilde{v}_r , \tilde{v}_z , \tilde{p} , and \tilde{h} remain identical to the low- k analysis presented in Sec. IV, the governing equations, kinematic condition, and no-slip conditions at $O(1)$ and $O(k)$ remain unchanged [i.e., Eqs. (A1a)–(A1c) are same as Eqs. (18)–(20) in Sec. IV, and Eq. (A2) here is identical to Eq. (23) in Sec. IV]. However, we write down these equations again for the sake of completeness of the present analysis, and more importantly, to point out the differences in present analysis and low- k analysis given previously in Sec. IV for capturing eigenvalue of the surfactant mode. The governing equation at leading order and $O(k)$ are

$$d_r \tilde{v}_r^{(j)} + \frac{1}{r} \tilde{v}_r^{(j)} + i \tilde{v}_z^{(j)} = 0, \quad (\text{A1a})$$

$$d_r \tilde{p}^{(j)} = 0, \quad (\text{A1b})$$

$$i \tilde{p}^{(j)} - d_r^2 \tilde{v}_z^{(j)} - \frac{1}{r} d_r \tilde{v}_z^{(j)} = 0, \quad (\text{A1c})$$

where superscript index $j = 0$ for leading order and $j = 1$ for equations correct up to $O(k)$. In a similar manner, the no-slip conditions at $r = S$ can be written as

$$\tilde{v}_z^{(j)} = 0, \quad \tilde{v}_r^{(j)} = 0. \quad (\text{A2})$$

The leading-order surfactant transport equation, kinematic condition, tangential, and normal stress balance are given as

$$d_r \tilde{v}_r^{(0)} = 0, \quad (\text{A3a})$$

$$\tilde{v}_r^{(0)} - i(\tilde{v}_z - c^{(0)})\tilde{h}^{(0)} = 0, \quad (\text{A3b})$$

$$d_r \tilde{v}_z^{(0)} + \tilde{h}^{(0)}(d_r^2 \tilde{v}_z) + iM\tilde{\Gamma}^{(0)} = 0, \quad (\text{A3c})$$

$$\tilde{p}^{(0)} + \frac{M}{S+1}\tilde{\Gamma}^{(0)} = 0. \quad (\text{A3d})$$

The surfactant transport equation, kinematic condition, tangential, and normal stress balance at $O(k)$ are

$$\underline{i(\tilde{v}_z - c^{(0)})\tilde{\Gamma}^{(0)}} = d_r \tilde{v}_r^{(1)}, \quad (\text{A4a})$$

$$\tilde{v}_r^{(1)} - i(\tilde{v}_z - c^{(0)})\tilde{h}^{(1)} + ic^{(1)}\tilde{h}^{(0)} = 0, \quad (\text{A4b})$$

$$\underline{d_r \tilde{v}_z^{(1)} + \tilde{h}^{(1)}(d_r^2 \tilde{v}_z) + iM\tilde{\Gamma}^{(1)}} = 0, \quad (\text{A4c})$$

$$\underline{\tilde{p}^{(1)} + \frac{\tilde{h}^{(0)}}{(S+1)^2} + \frac{M}{S+1}\tilde{\Gamma}^{(1)}} = 0. \quad (\text{A4d})$$

The underlined equations above represent the GL interfacial conditions at leading-order and first correction which are

modified due to different scalings used in the present analysis as compared to the interfacial conditions given in Sec. IV. The subsequent analysis reveals that calculations up to $O(k)$ are sufficient to capture the surfactant mode instability depicted in above neutral curves in low- k regime. The governing equations and boundary conditions at leading order are used to evaluate leading-order wave speed $c^{(0)}$ in the following manner. The leading-order r momentum Eq. (A1b) and normal stress balance [Eq. (A3d)] are used to find the leading-order pressure profile: $\tilde{p}^{(0)} = -M\tilde{\Gamma}^{(0)}/(S+1)$. Equation (A1c) is integrated and on using the no-slip condition ($\tilde{v}_z^{(0)} = 0$) at $r = S$, and leading-order tangential stress balance [Eq. (A3c)], we obtain

$$\tilde{v}_z^{(0)} = \text{Bo} \tilde{h}^{(0)} (1+S) \ln \left(\frac{r}{S} \right) - \frac{i \tilde{\Gamma}^{(0)} M}{4(1+S)} \left(r^2 - S^2 + 2(1+S)^2 \ln \frac{r}{S} \right). \quad (\text{A5})$$

The continuity equation [Eq. (A1a)] is then used along with no-slip condition to determine $\tilde{v}_r^{(0)}$. Similar to the expression of $\tilde{v}_z^{(0)}$ above, the expression of $\tilde{v}_r^{(0)}$ also contains two terms: one proportional to $\tilde{h}^{(0)}$ and other to $\tilde{\Gamma}^{(0)}$. The surfactant transport equation at leading order ($d_r \tilde{v}_r^{(0)} = 0$) is then used to evaluate $\tilde{\Gamma}^{(0)}$. This expression is of the form $\tilde{\Gamma}^{(0)} = \frac{\text{Bo} \tilde{h}^{(0)} g(S)}{M}$, where g is a function of S . This in turn implies that the expression of $\tilde{v}_z^{(0)}$ and $\tilde{v}_r^{(0)}$ will be proportional to $\tilde{h}^{(0)}$. The kinematic condition at leading order [Eq. (A3b)] is finally used to determine leading-order wave speed $c^{(0)}$. The leading-order wave speed is found to be real, and hence, we proceed to calculations at next correction to find the expression of $c^{(1)}$. The sequence of steps involved in finding $c^{(1)}$ are identical to the sequence used in obtaining leading-order wave speed. The eigenvalue correct up to $O(k)$ is

$$c = c^{(0)} + kc^{(1)} = \text{Bo} \zeta_1 + ik \frac{q_2}{q_1} \left[1 - \frac{\text{Bo}^2}{64M} \frac{g_1}{(1+S)^6 q_1^2} \right], \quad (\text{A6})$$

where ζ_1 , q_1 , and q_2 are positive values functions of S and are given in Appendix B. The above equation shows that the first correction to wave speed is imaginary, and setting it equal to zero gives the expression of M . Thus, the expression of critical Marangoni number as a function of k can be written using $\text{Ma}_{\text{crit}} = M/k^2$,

$$\text{Ma}_{\text{crit}} = \frac{\text{Bo}^2}{64k^2} \frac{g_1}{(1+S)^6 q_1^2}, \quad (\text{A7})$$

where $g_1(S)$ and $q_1(S)$ are given in Appendix B.

APPENDIX B: FUNCTIONS APPEARING IN ANALYTICAL RESULTS

In this Appendix, we provide all the functions of S that appear in analytical solutions in asymptotic analysis:

$$A_1 = \left[(S+1)^2 - S^2 + 2(S+1)^2 \ln \left(\frac{S+1}{S} \right) \right], \quad A_2 = \left[(S+1)^4 - S^4 - 4(S+1)^4 \ln \left(\frac{S+1}{S} \right) \right],$$

$$q = - \left[\frac{A_2 + 8S^2 + 8S + 2}{16(S+1)^3} \right], \quad n = - \left[\frac{A_1 A_2}{16(S+1)^3 f} \right], \quad \text{where } f = f(r) |_{r=S+1} \text{ with } f(r) \text{ defined in Sec. IV in Eq. (16).}$$

$$\zeta = \left\{ \frac{(1+2S)[(1+2S) + (1+2S+2S^2)\ln(\frac{S}{S+1})]}{4[(1+2S)(S+1) + 2(S+1)^3\ln(\frac{S}{S+1})]} \right\},$$

$$\zeta_1 = \frac{1}{4} \left\{ 2(1+S)^2 \ln\left(\frac{S+1}{S}\right) - \frac{(1+2S)[9+36S+46S^2+20S^3-4S^2(1+S)^2\ln(\frac{S+1}{S})]}{[5+20S+26S^2+12S^3+4(1+S)^4\ln(\frac{S+1}{S})]} \right\},$$

$$q_1 = \left\{ \frac{[(5+20S+26S^2+2S^3)+4(S+1)^4\ln(\frac{S+1}{S})]}{16(S+1)^3} \right\},$$

$$q_2 = - \left\{ \frac{(1+3S+2S^2)[1+2S+(1+2S+2S^2)\ln(\frac{S}{S+1})]}{4(S+1)^3} \right\},$$

$$g_1 = (S+1)^4 \left(-[(1+2S)^2(1+2S+2S^2)] + 8(S+1)^6 \{ \ln[S(S+1)] \}^2 + 2(S+1)^2(1+2S)^2 \ln\left(\frac{S+1}{S}\right) - 16(S+1)^6 \ln S \ln(S+1) \right),$$

-
- [1] S. L. Goren, The instability of an annular liquid thread, *J. Fluid Mech.* **12**, 309 (1962).
- [2] S. P. Lin and W. C. Liu, Instability of film coating of wires and tubes, *AIChE J.* **21**, 775 (1975).
- [3] W. B. Krantz and R. L. Zollars, The linear hydrodynamic stability of film flow down a vertical cylinder, *AIChE J.* **22**, 930 (1976).
- [4] F. J. Solorio and M. Sen, Linear stability of cylindrical falling film, *J. Fluid Mech.* **183**, 365 (1987).
- [5] C. S. Yih, Stability of liquid flow down an inclined plane, *Phys. Fluids* **6**, 321 (1963).
- [6] A. L. Frenkel, Nonlinear theory of strongly undulating thin films flowing down vertical cylinders, *Europhys. Lett.* **18**, 583 (1992).
- [7] S. Kalliadasis and H. C. Chang, Drop formation during coating of vertical fibres, *J. Fluid Mech.* **261**, 135 (1994).
- [8] H. C. Chang and E. A. Demekhin, Mechanism for drop formation on a coated vertical fibre, *J. Fluid Mech.* **380**, 233 (1999).
- [9] I. L. Kliakhandler, S. H. Davis, and S. G. Bankoff, Viscous beads on vertical fibre, *J. Fluid Mech.* **429**, 381 (2001).
- [10] R. V. Craster and O. K. Matar, On viscous beads flowing down a vertical fibre, *J. Fluid Mech.* **553**, 85 (2006).
- [11] G. M. Sisev, R. V. Craster, O. K. Matar, and S. V. Gerasimov, Film flow down a fibre at moderate flow rates, *Chem. Eng. Sci.* **61**, 7279 (2006).
- [12] C. Duprat, C. Ruyer-Quil, S. Kalliadasis, and F. Giorgiutti-Dauphiné, Absolute and Convective Instabilities of a Viscous Film Flowing Down a Vertical Fiber, *Phys. Rev. Lett.* **98**, 244502 (2007).
- [13] C. Ruyer-Quil, P. Treveleyan, F. Giorgiutti-Dauphiné, C. Duprat, and S. Kalliadasis, Modelling film flows down a fiber, *J. Fluid Mech.* **603**, 431 (2008).
- [14] L. B. Smolka, J. North, and B. K. Guerra, Dynamics of free surface perturbations along an annular viscous film, *Phys. Rev. E* **77**, 036301 (2008).
- [15] A. G. Gonzalez, J. A. Diez, R. Gratton, D. M. Campana, and F. A. Saita, Instability of a viscous liquid coating a cylindrical fibre, *J. Fluid Mech.* **651**, 117 (2010).
- [16] C. Ruyer-Quil and S. Kalliadasis, Wavy regimes of film flow down a fiber, *Phys. Rev. E* **85**, 046302 (2012).
- [17] L. Yu and J. Hinch, The velocity of large viscous drops falling on a coated vertical fibre, *J. Fluid Mech.* **737**, 232 (2013).
- [18] H. Ji, C. Falcon, A. Sadeghpour, Z. Zeng, Y. S. Ju, and A. L. Bertozzi, Dynamics of thin liquid films on vertical cylindrical fibres, *J. Fluid Mech.* **865**, 303 (2019).
- [19] K. J. Cassidy, D. Halpern, B. G. Ressler, and J. B. Grothberg, Surfactant effects in model airway closure experiments, *J. Appl. Physiol.* **87**, 415 (1999).
- [20] D. M. Camapana, J. Di Paolo, and F. A. Saita, A 2D model of Rayleigh instability in capillary tubes: Surfactant effects, *Int. J. Multiphase Flow* **30**, 431 (2004).
- [21] D. Halpern and J. Grothberg, Surfactant effects on fluid-elastic instabilities of liquid-lined flexible tubes: A model of airway closure, *J. Biomech Eng.* **115**, 271 (1993).
- [22] D. R. Otis, M. J. Johnson, T. J. Pedley, and R. D. Kamm, Role of pulmonary surfactant in airway closure: A computational study, *J. Appl. Physiol.* **75**, 1323 (1993).
- [23] B. J. Carroll and J. Lucassen, Effect of surface dynamics on the process of droplet formation from supported and free liquid cylinders, *Chem. Soc. Faraday Trans.* **70**, 1228 (1974).
- [24] H.-H. Wei, Stability of a viscoelastic falling film with surfactant subjected to interfacial shear, *Phys. Rev. E* **75**, 036306 (2007).
- [25] L. Preziosi, K. P. Chen, and D. D. Joseph, Lubricated pipelining: Stability of core-annular flow, *J. Fluid Mech.* **201**, 323 (1989).
- [26] Gaurav and V. Shankar, Manipulation of instabilities in core-annular flows using a deformable solid layer, *Phys. Fluids* **25**, 014104 (2013).
- [27] A. L. Frenkel and D. Halpern, Stokes-flow instability due to interfacial surfactant, *Phys. Fluids* **14**, L45 (2002).
- [28] D. Halpern and A. L. Frenkel, Destabilization of a creeping flow by interfacial surfactant: Linear theory extended to all wave numbers, *J. Fluid Mech.* **485**, 191 (2003).
- [29] M. G. Blyth and C. Pozrikidis, Effect of surfactant on the stability of flow down an inclined plane, *J. Fluid Mech.* **521**, 241 (2004).

- [30] M. G. Blyth, H. Luo, and C. Pozrikidis, Stability of axisymmetric core-annular flow in the presence of an insoluble surfactant, *J. Fluid Mech.* **548**, 207 (2006).
- [31] A. P. Bassom, M. G. Blyth, and D. T. Papageorgiou, Using surfactants to stabilize two-phase pipe flows of core-annular type, *J. Fluid Mech.* **704**, 333 (2012).
- [32] M. G. Blyth and A. P. Bassom, Stability of surfactant-laden core-annular flow and rod-annular flow to nonaxisymmetric modes, *J. Fluid Mech.* **716**, 716 R13 (2013).
- [33] H.-H. Wei, Effect of surfactant on the long-wave instability of a shear-imposed liquid flow down an inclined plane, *Phys. Fluids* **17**, 012103 (2005).
- [34] L. G. Leal, *Advanced Transport Phenomena: Fluid Mechanics and Convective Transport Processes*, Cambridge Series in Chemical Engineering (Cambridge University Press, Cambridge, 2010).
- [35] H. A. Stone, A simple derivation of the time-dependent convective-diffusion equation for surfactant transport along a deforming interface, *Phys. Fluids A: Fluid Dynam.* **2**, 111 (1990).
- [36] D. Vitasari, P. Grassia, and P. Martin, Surfactant transport onto a foam lamella, *Chem. Eng. Sci.* **102**, 405 (2017).
- [37] R. B. Bird, W. E. Stewart, and E. N. Lightfoot, *Transport Phenomena*, 2nd ed. (Wiley, New York, 2009).
- [38] D. S. Tomar, M. Baingne, and G. Sharma, Stability of gravity-driven free surface flow of surfactant-laden liquid film flowing down a flexible inclined plane, *Chem. Eng. Sci.* **165**, 216 (2017).
- [39] J. Eggers and E. Villermaux, Physics of liquid jets, *Rep. Progress Phys.* **71**, 036601 (2008).
- [40] F. Gallaire and P. T. Brun, Fluid dynamic instabilities: Theory and application to pattern forming in complex media, *Phil. Trans. R. Soc. A* **375**, 20160155 (2017).
- [41] D. Halpern and H. H. Wei, Slip-enhanced drop formation in a liquid falling down a vertical fibre, *J. Fluid Mech.* **820**, 42 (2017).
- [42] Z.-Q. Zhou, J. Peng, Y.-J. Zhang, and W.-L. Zhuge, Instabilities of viscoelastic liquid film coating tube in the presence of surfactant, *J. Non-Newtonian Fluid Mech.* **204**, 94 (2014).
- [43] H.-H. Wei, On the flow-induced marangoni instability due to the presence of surfactant, *J. Fluids Mech.* **544**, 173 (2005).
- [44] A. Pereira and S. Kalliadasis, Dynamics of a falling film with solutal Marangoni effect, *Phys. Rev. E* **78**, 036312 (2008).